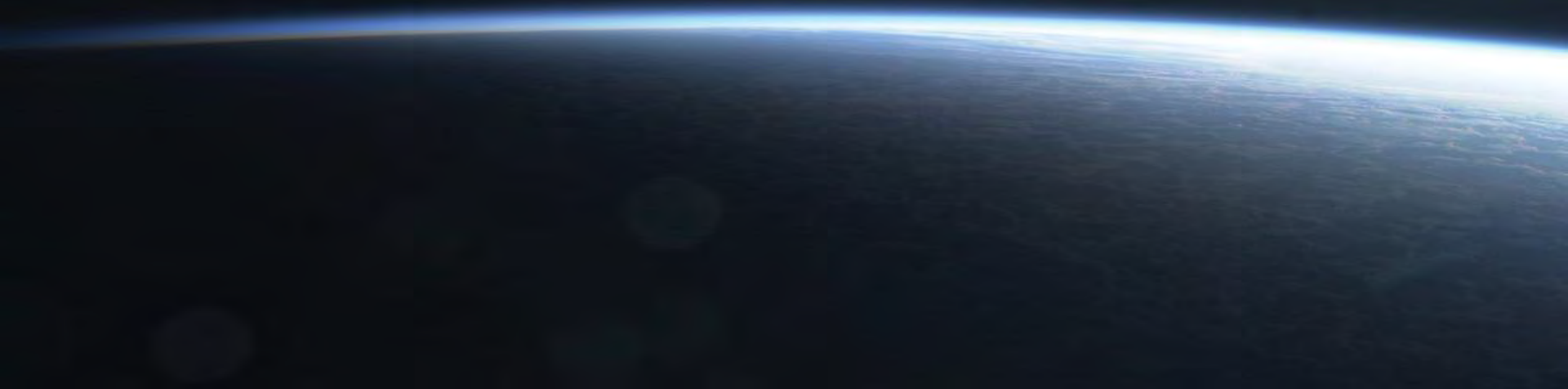


# ESA Earth Explorers

*Diego Fernandez-Prieto  
Head of the Research & Development Section  
European Space Agency*



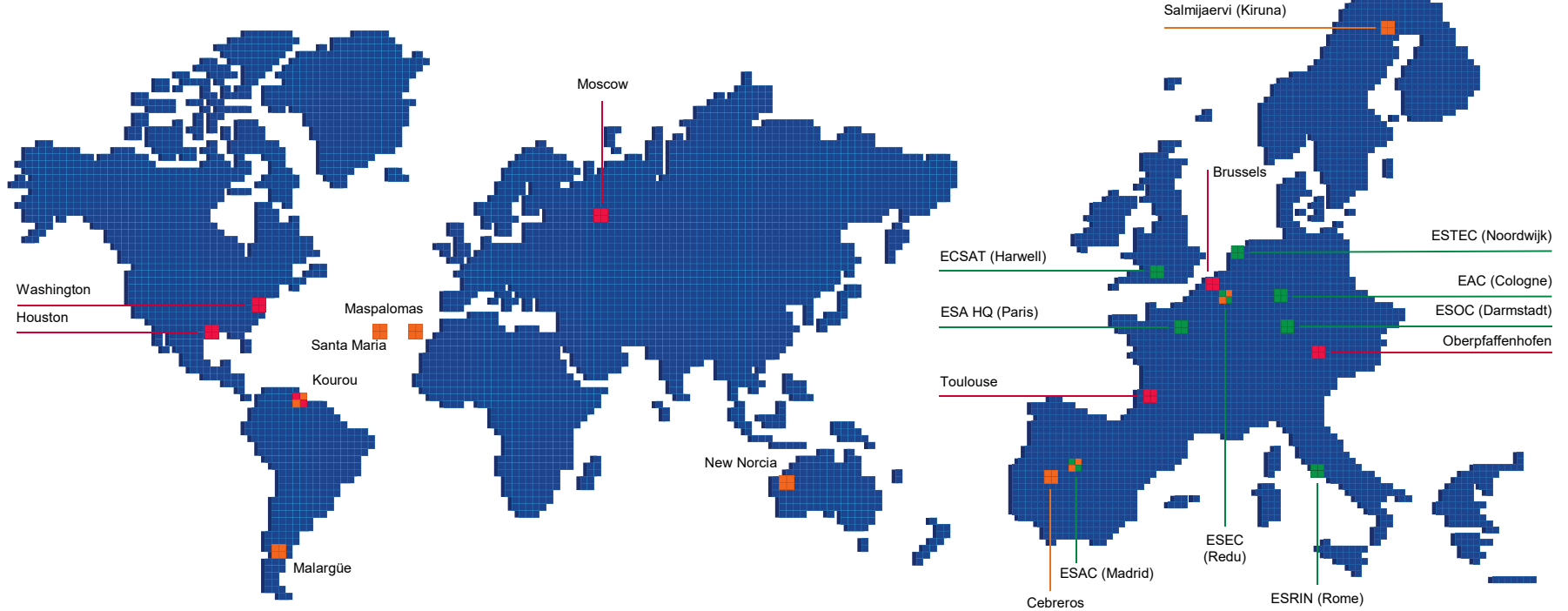
## Purpose of ESA & Its Member States



“To provide for and promote, for exclusively peaceful purposes, cooperation among European states in space research and technology and their space applications.”

Article 2 of ESA Convention

# ESA's locations



- ESA sites
- Offices
- ESA Ground Station
- ESA Ground Station + Offices
- ESA sites + ESA Ground Station

ESA UNCLASSIFIED - For Official Use



ESA is one of the few space agencies in the world to combine responsibility in nearly all areas of space activity.

\* Space science is a Mandatory programme, all Member States contribute to it according to GNP. All other programmes are Optional, funded 'a la carte' by Participating States.



space science



human spaceflight



exploration



earth observation



space transportation



navigation



operations



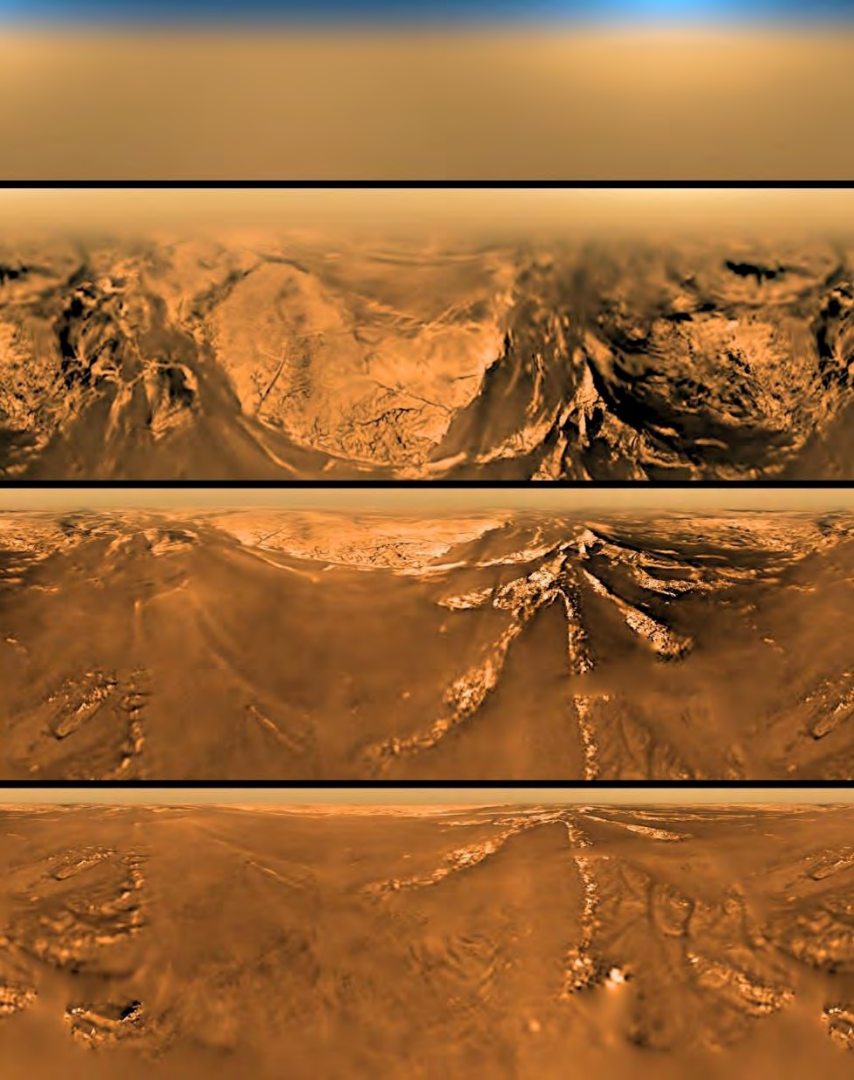
technology



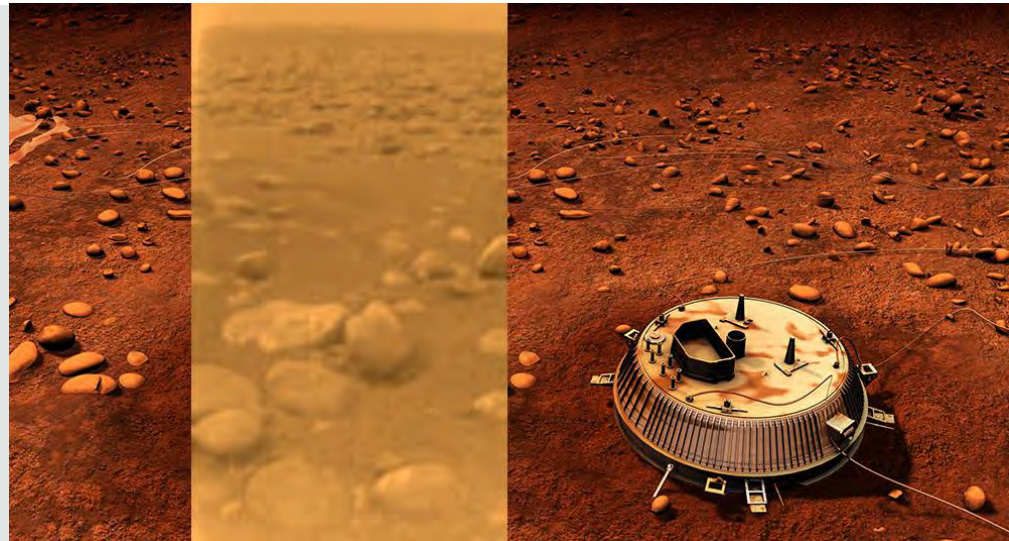
telecommunications



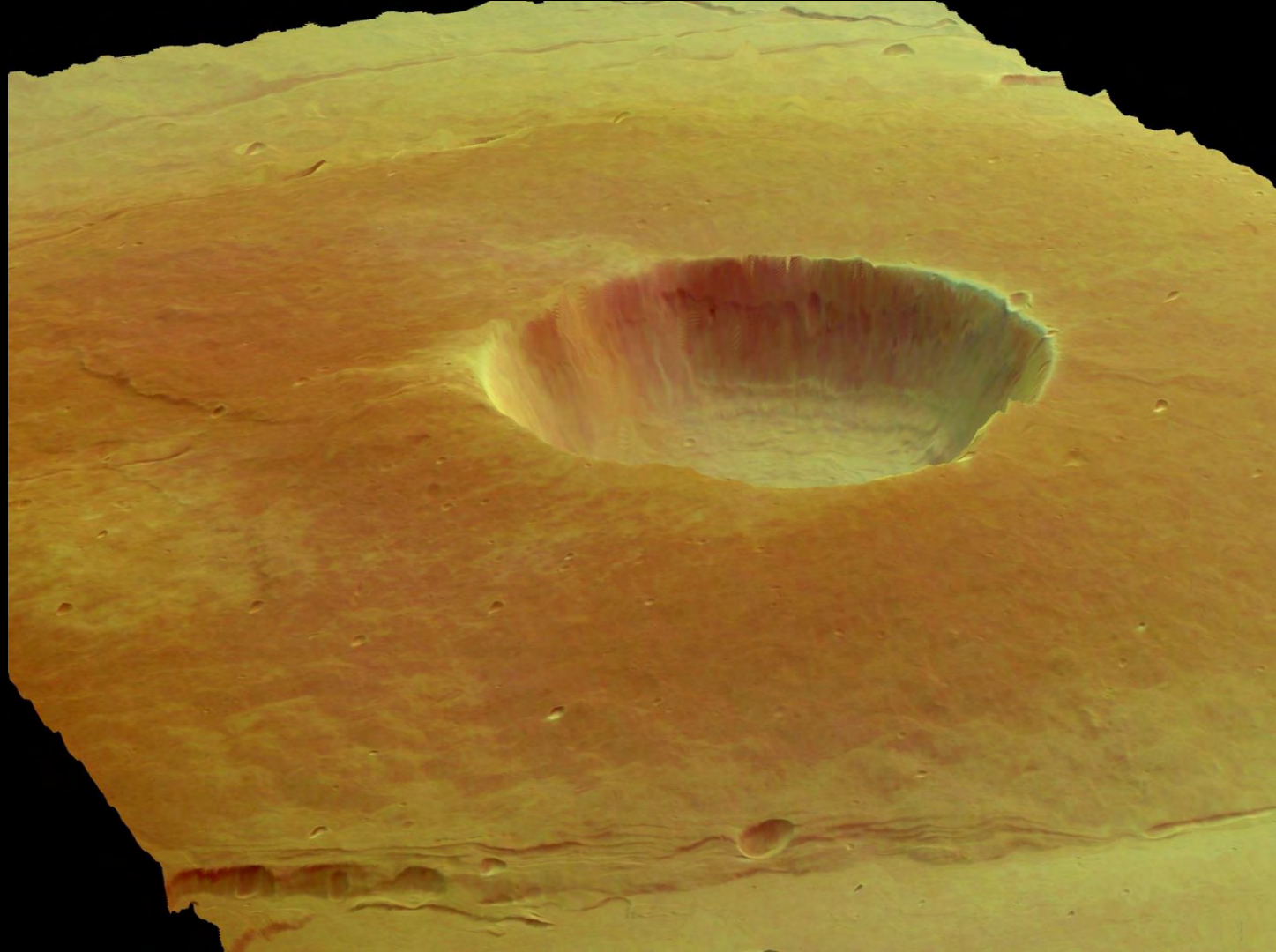




tem







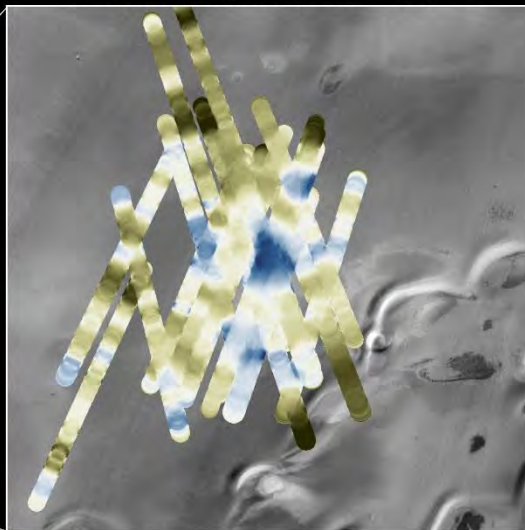


# Mars Express

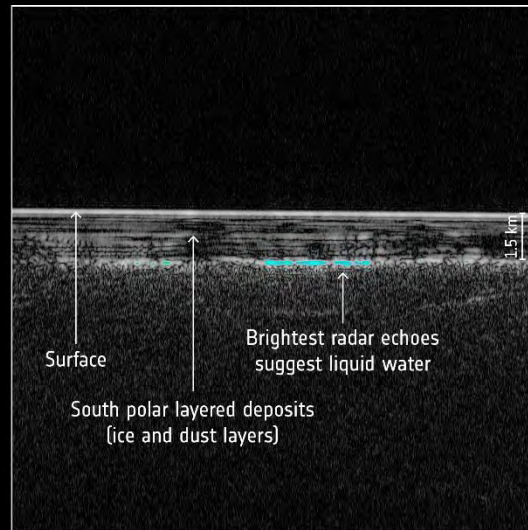
Mars south polar region

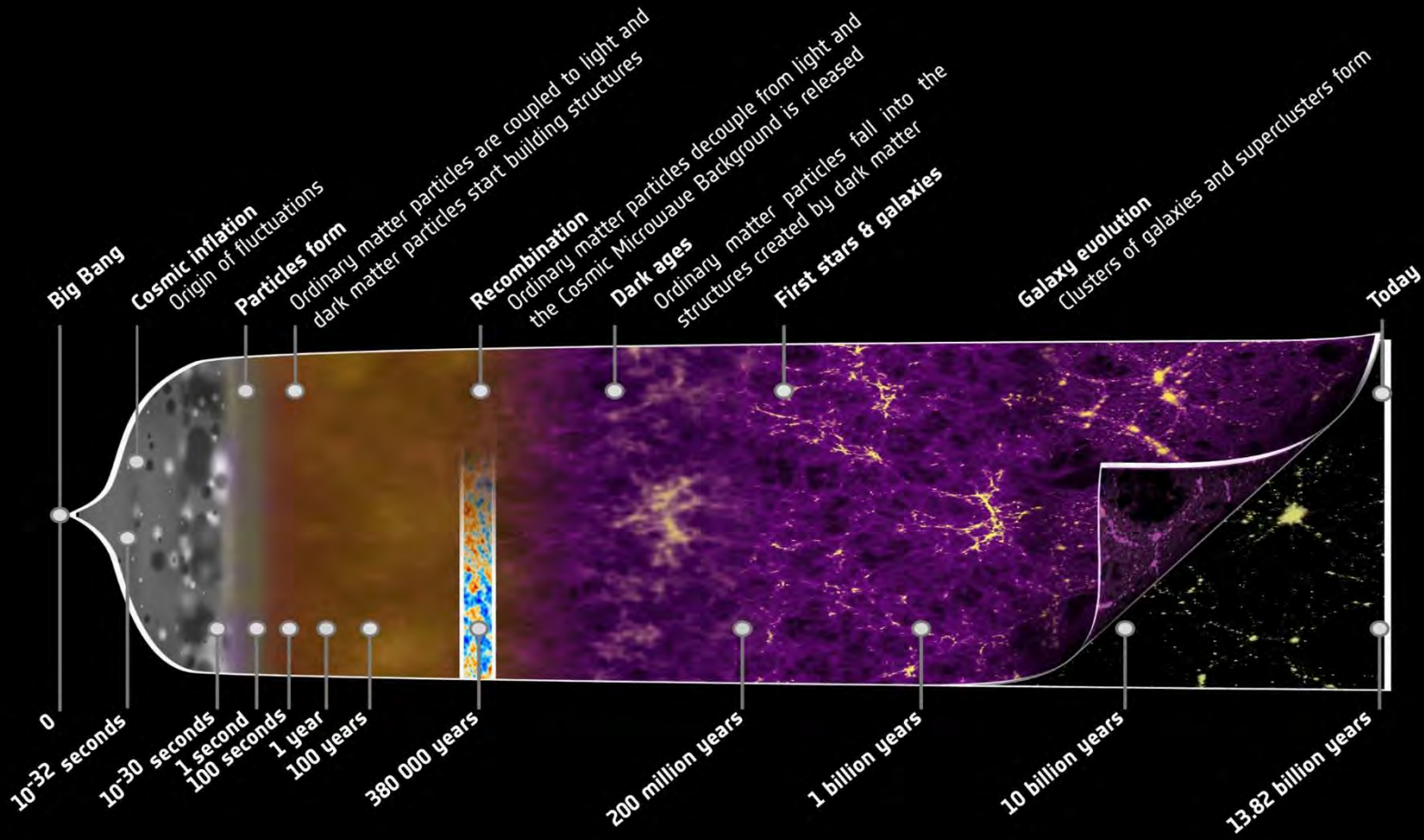


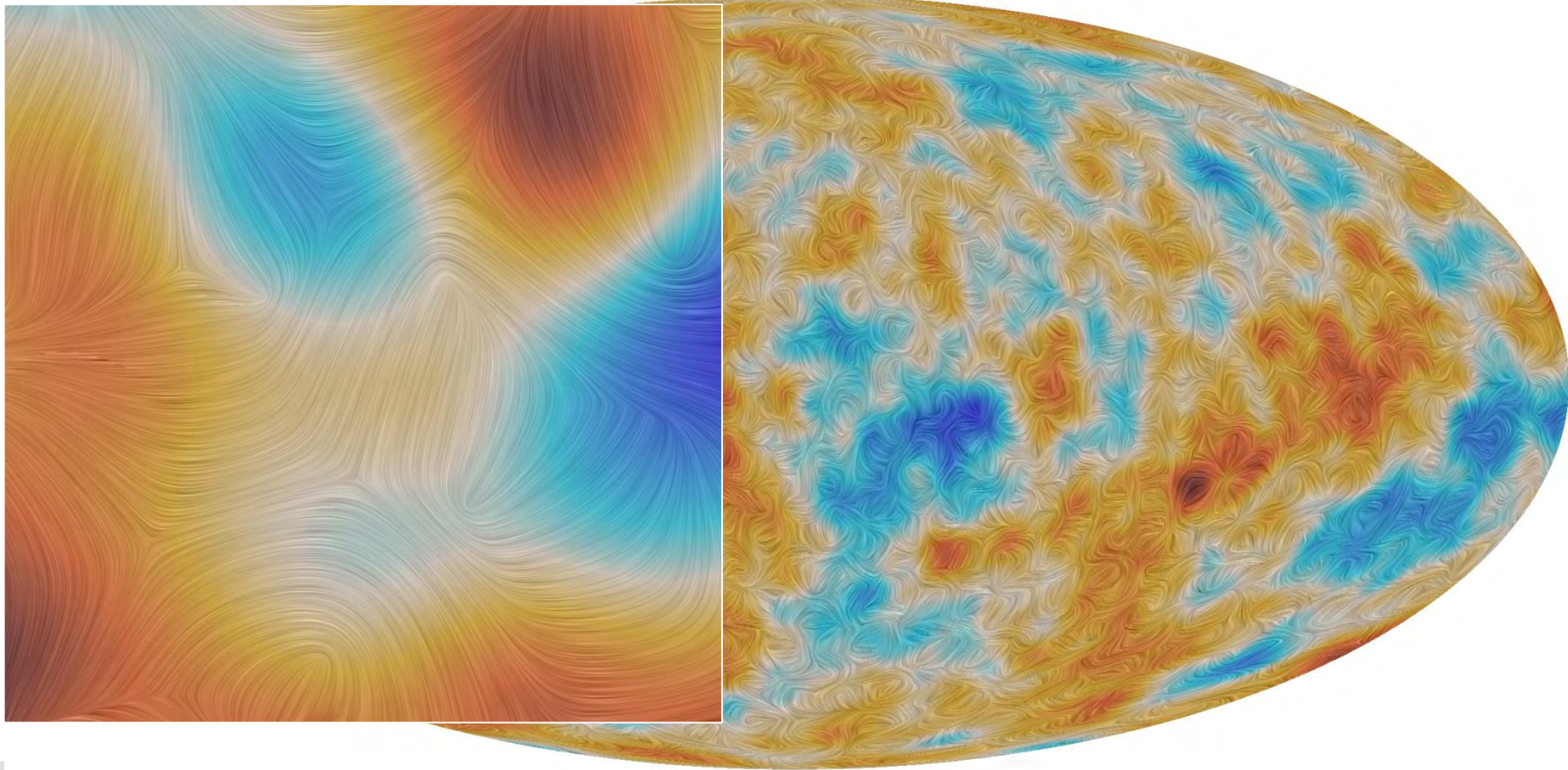
Mars Express radar footprints  
(blue = brightest radar echo)



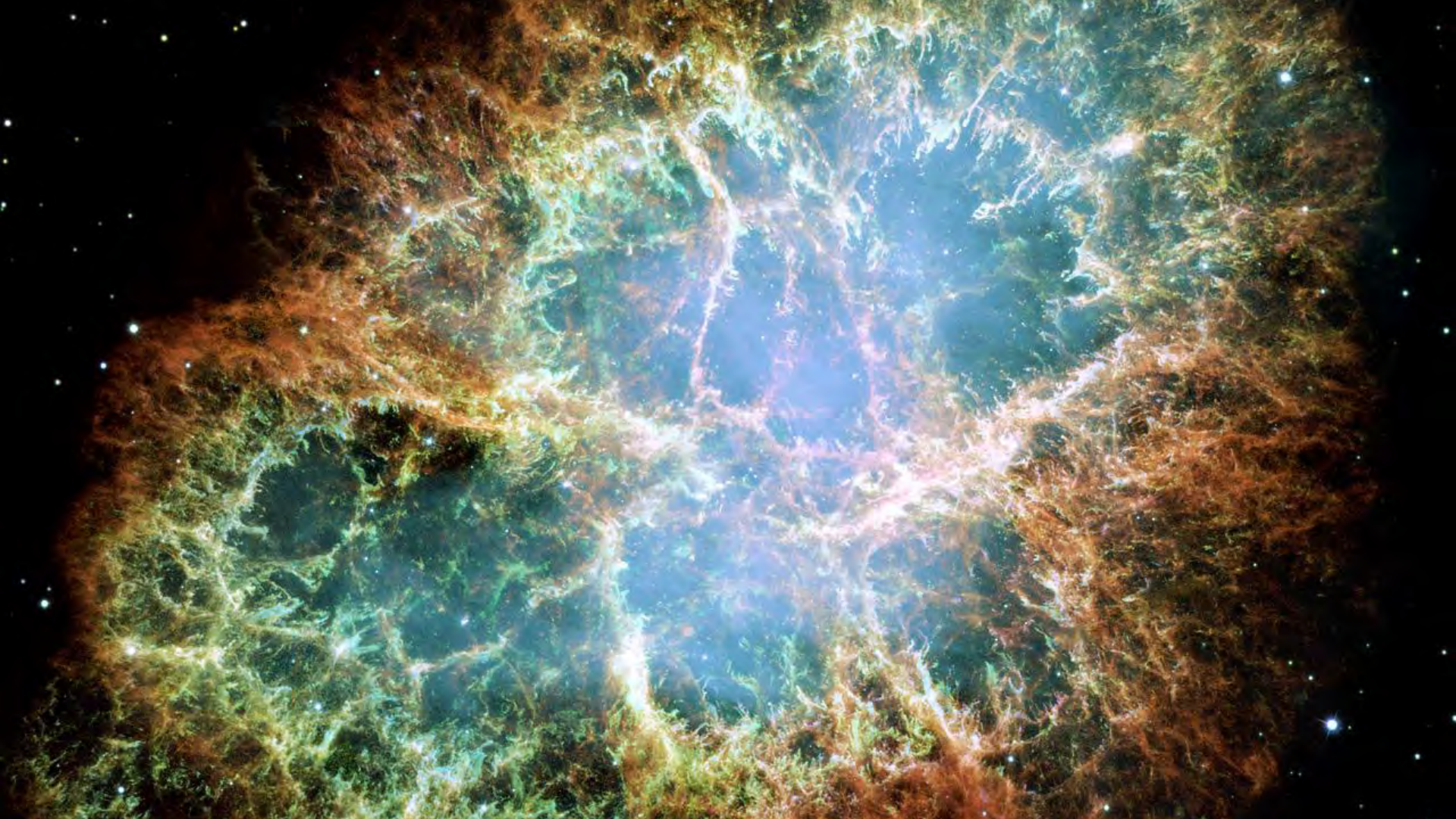
Radar image of subsurface

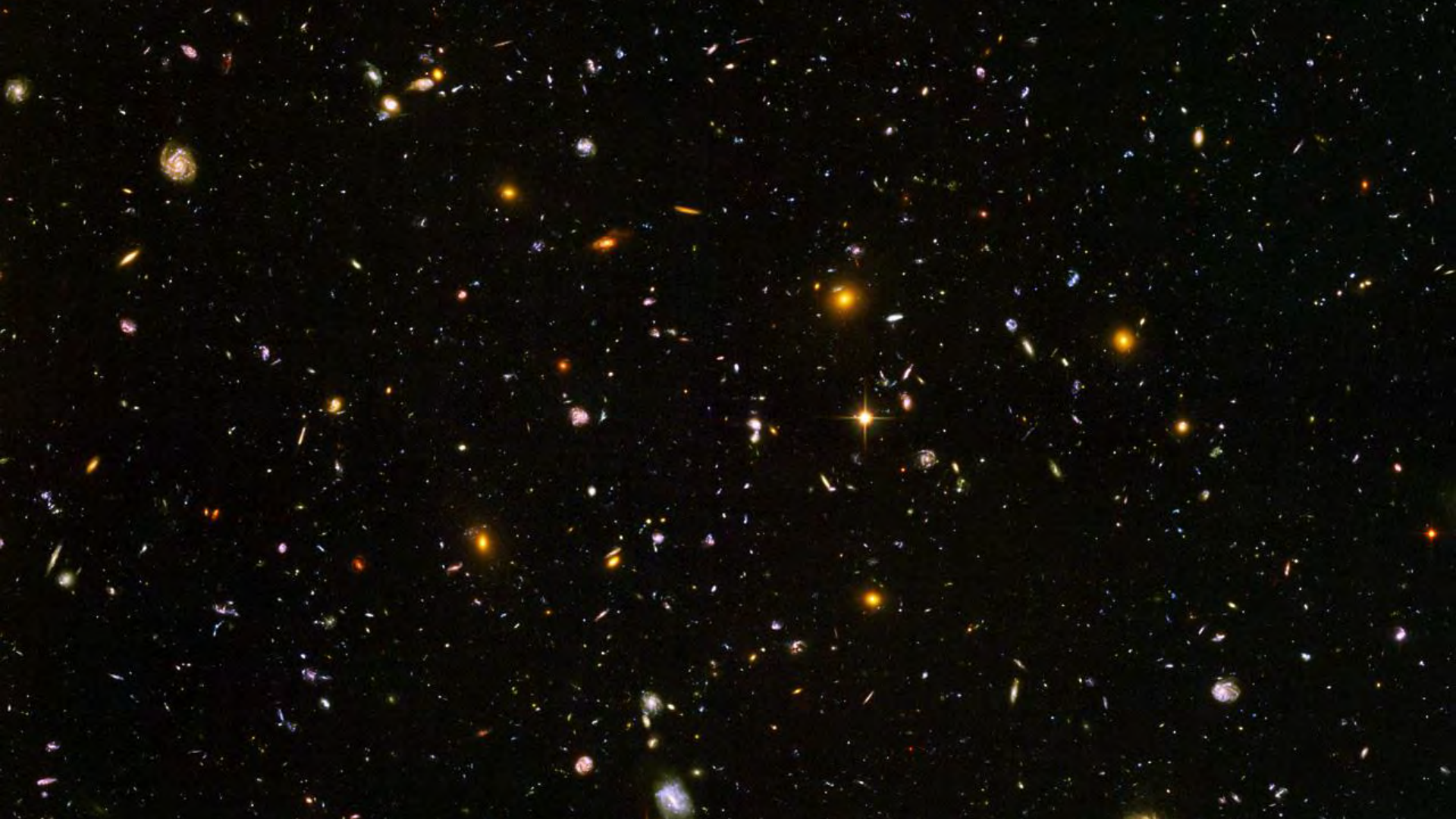
















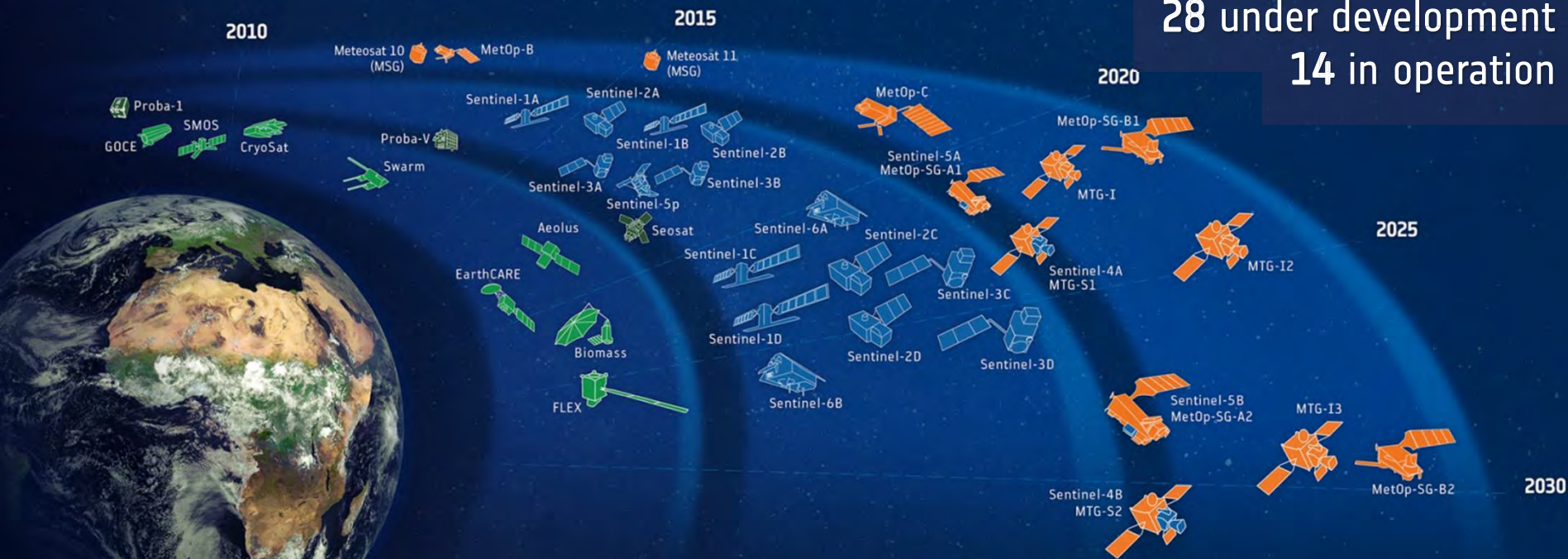
# ESA-DEVELOPED EARTH OBSERVATION MISSIONS



Satellites

28 under development

14 in operation

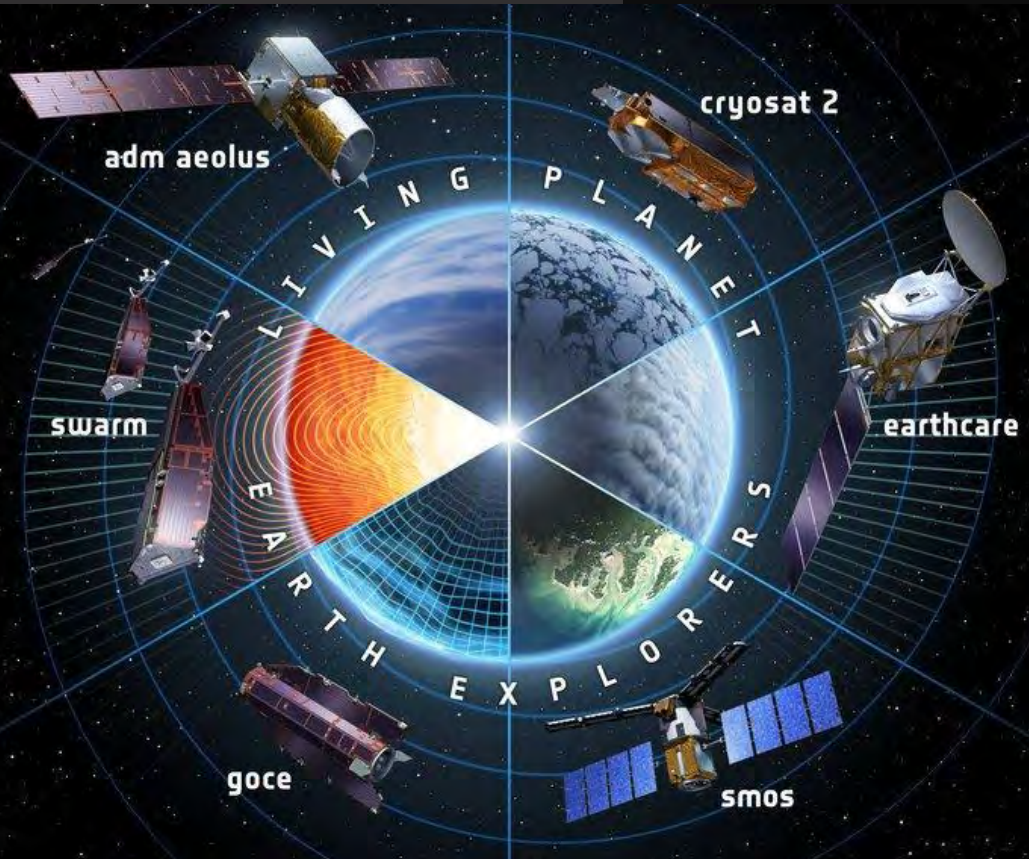


Science

Copernicus

Meteorology

# Earth Explorers



**GOCE**

**2009 – 2013**

**SMOS**

**2009 – Present**

**Cryosat**

**2010 – Present**

**SWARM**

**2013 – Present**

**Aeolus**

**2018**

**EarthCARE**

**2020**

**Biomass**

**2021**

**FLEX**

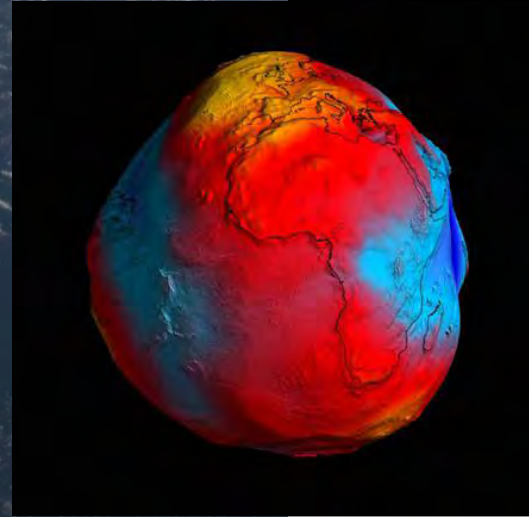
**2022**



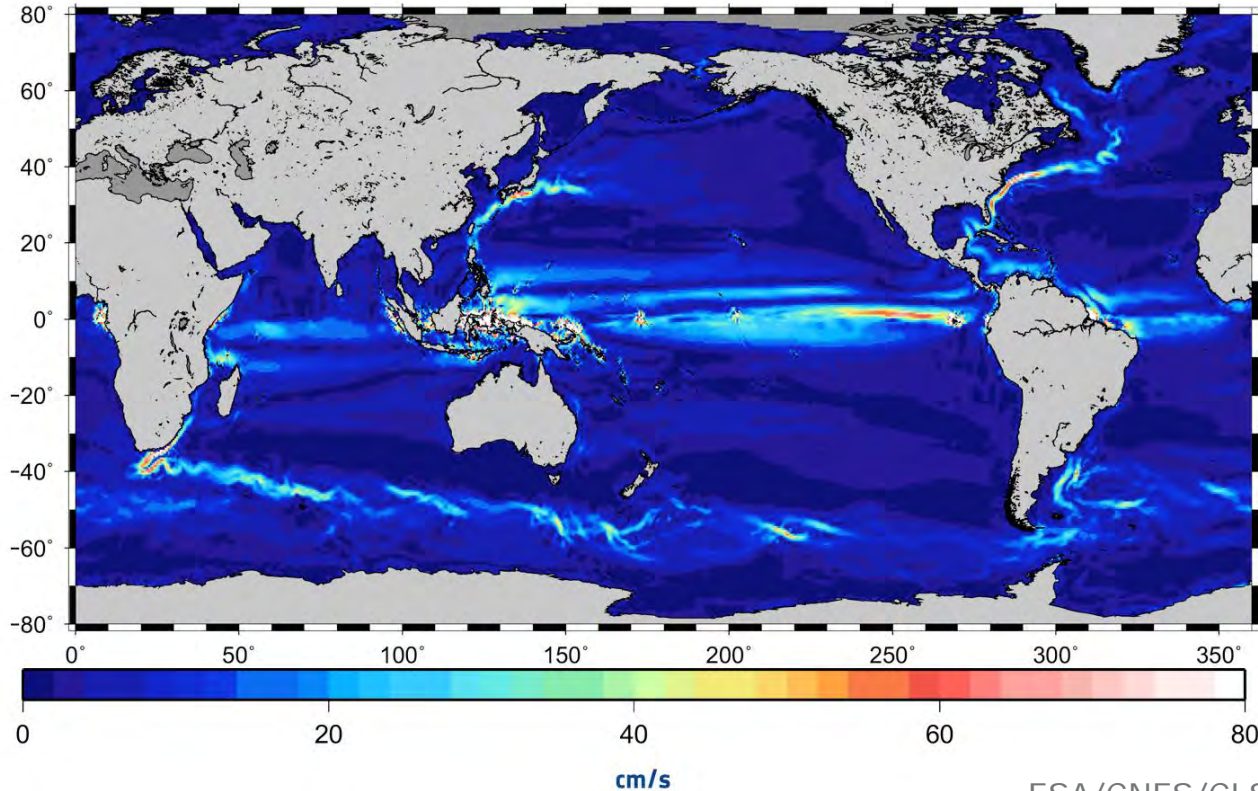
# GOCE: ESA's Gravity Field and Steady-state Ocean Circulation Explorer



- First gradiometer in space launched 17 March 2009
- Best ever static geoid
- 5<sup>th</sup> version of geoid released in July 2014, including all GOCE measurements
- News on 6<sup>th</sup> release this week! (wed & thurs - geodesy)
- End of mission declared 21 October 2013 following depletion of Xenon fuel
- Re-entry 11 November 2013



# GOCE & Altimetry: Global Mean Ocean Currents



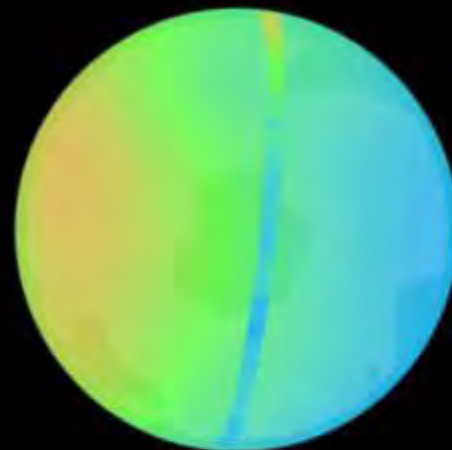
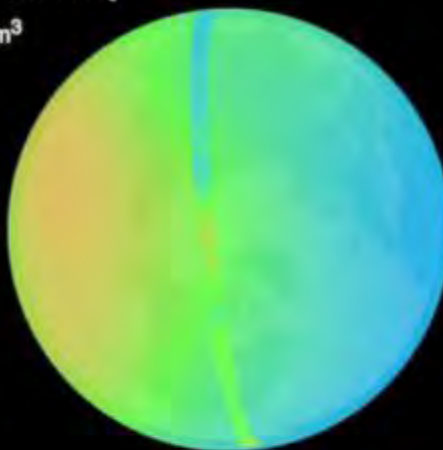
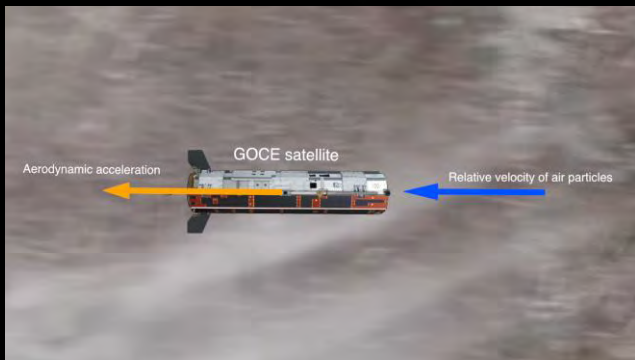
Altimetry derived mean sea surface when combined with GOCE geoid gives the “mean dynamic topography” (MDT)

MDT is the relief or shape of the ocean surface corresponding to mean ocean circulation

GOCE geoid contributing to the fundamental understanding of role of global ocean circulation in distributing heat and freshwater/salt.

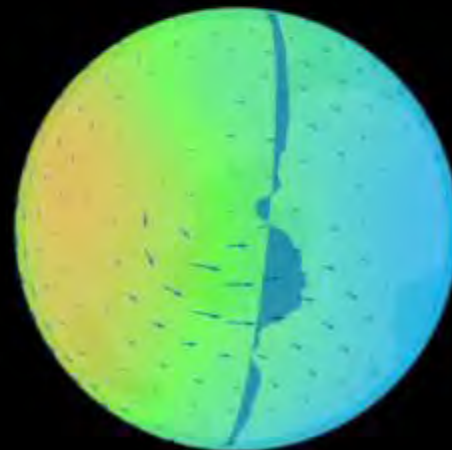
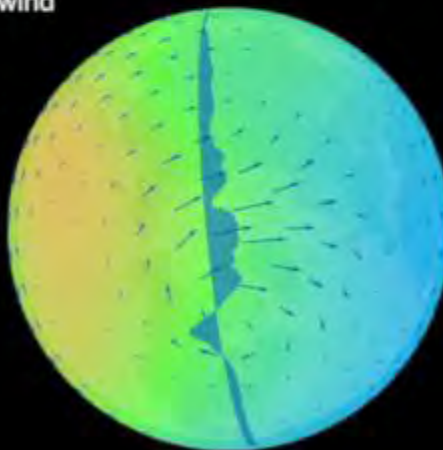


### GOCE density / NRLMSISE-00 model density



### GOCE crosswind / HWM-07 model wind

→ 300 m/s



2010-04-01 00:00







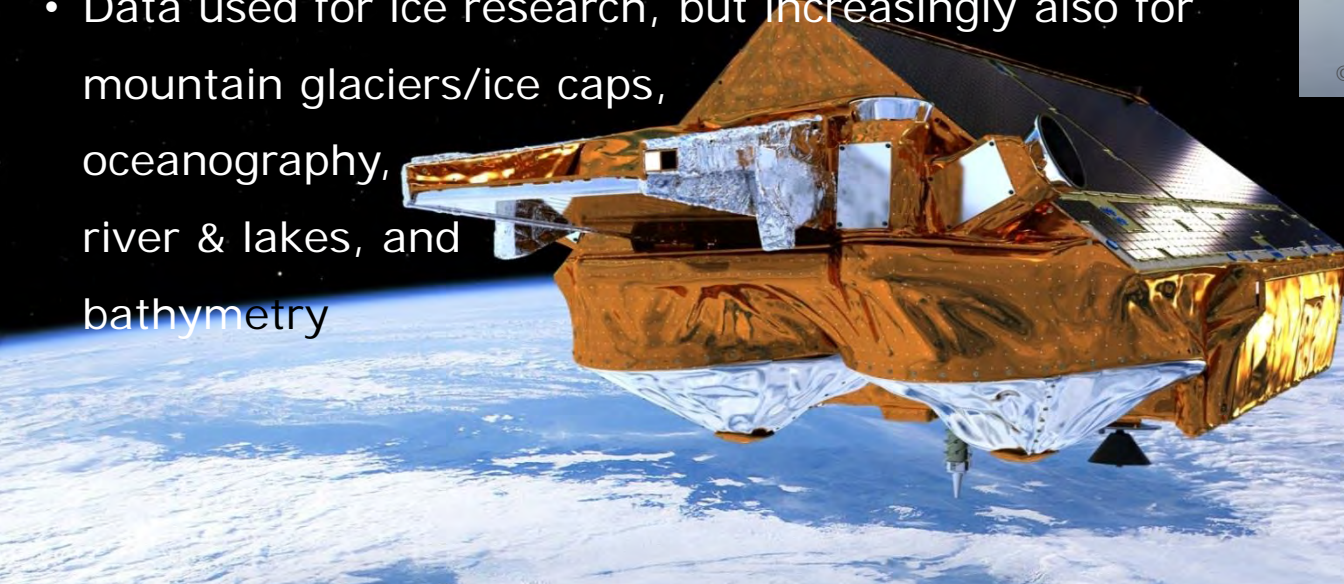
# CryoSat: ESA's Ice Mission



- Launched 08 April 2010
- First interferometric altimeter in space
- Global ice elevation & thickness change measurements
- Data used for ice research, but increasingly also for mountain glaciers/ice caps, oceanography, river & lakes, and bathymetry



© Thinkstock by Getty Images



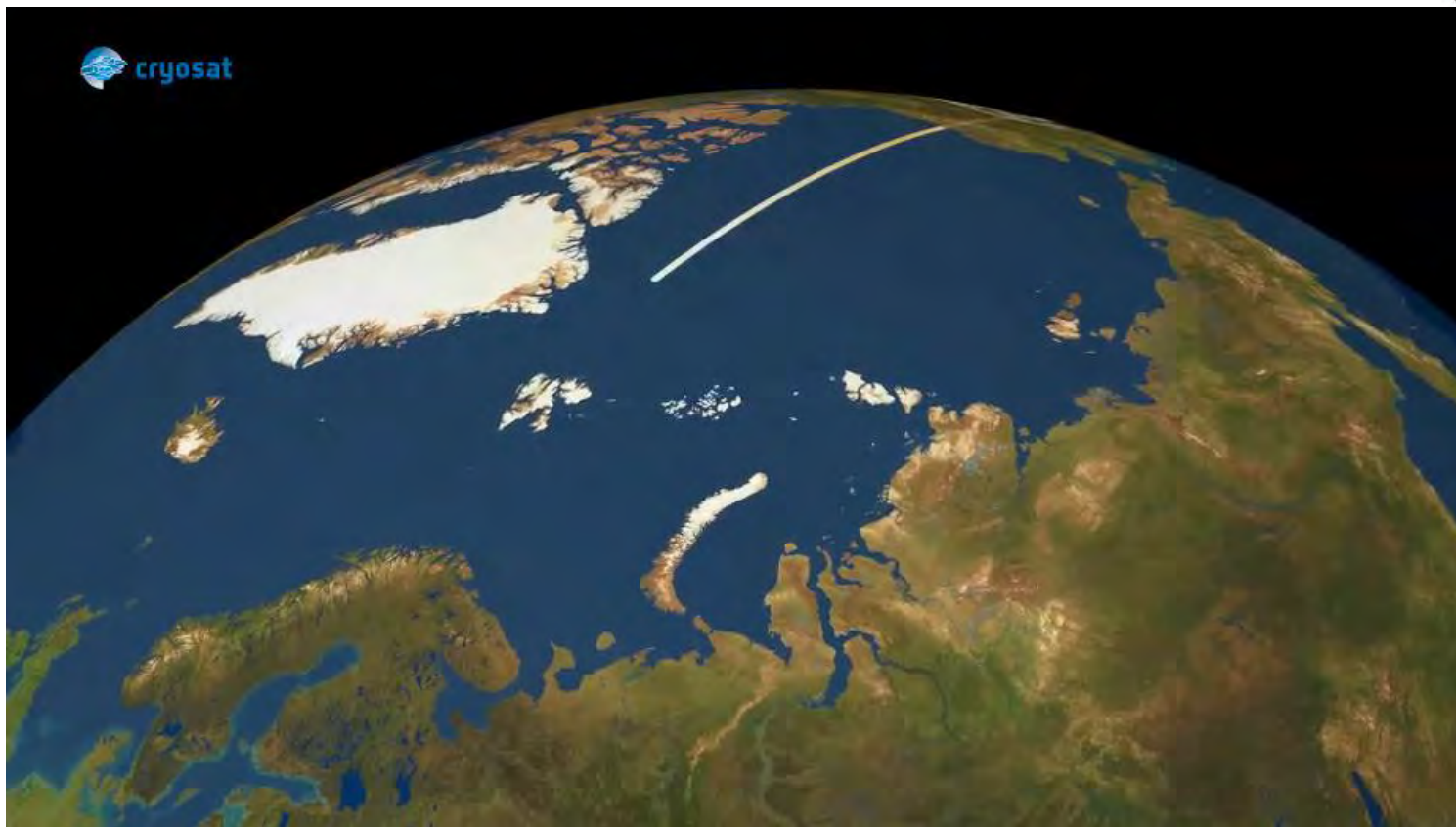
# CryoSat: Sea Ice Thickness & Volume



- Autumn 2010 - 2013, reduction in Arctic sea ice volume consistent with change in extent
- Replenishment in ice volume from 2013 – 2014 indicating resilience but large multi-year oscillation
- Recent decline from 2014 – 2016 with anomalously low cumulative growth in autumn 2016



# CryoSat: MDT & Currents

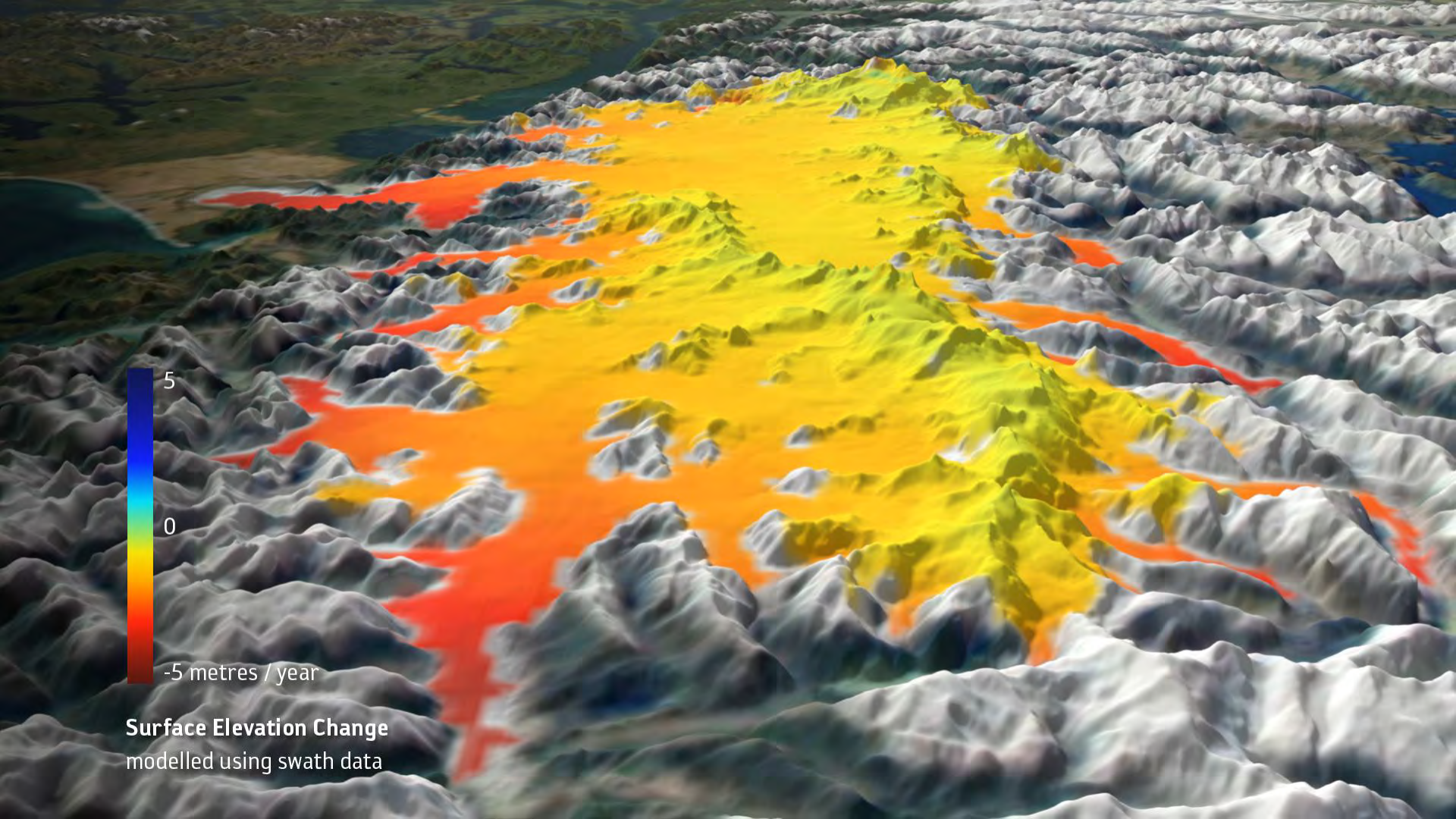




**STSE CryoTop:**  
First Greenland DEM at 500m pacing by exploiting the SARIN swath processing potential of CryoSat;

**SARIN Swath processing technique:**

- Enhance the number of elevation samples by several orders of magnitude;
- Enhance DEM resolution down to <500m;
- Allows retrieval of elevation on areas uncovered by traditional altimetry



5

0

-5 metres / year

Surface Elevation Change  
modelled using swath data



## Connected subglacial lake drainage beneath Thwaites Glacier, West Antarctica

Benjamin E. Smith<sup>1</sup>, Noel Gourmelen<sup>2,3</sup>, Alexander Huth<sup>4</sup>, and Ian Joughin<sup>1</sup>

<sup>1</sup>Applied Physics Lab, University of Washington, Seattle, WA 98195, USA

<sup>2</sup>School of Geosciences, University of Edinburgh, Edinburgh, EH8, Scotland

<sup>3</sup>IPGS UMR 7516, Université de Strasbourg, CNRS, Strasbourg, France

<sup>4</sup>Department of Earth and Space Sciences, University of Washington, Seattle, WA 98195, USA

Correspondence to: Benjamin E. Smith (bsmith@apl.washington.edu)

Received: 16 July 2016 – Discussion started: 28 July 2016

Revised: 24 November 2016 – Accepted: 3 January 2017 – Published: 8 February 2017

**Abstract.** We present conventional and swath altimetry data from CryoSat-2, revealing a system of subglacial lakes that drained between June 2013 and January 2014 under the central part of Thwaites Glacier, West Antarctica (TWG). Much of the drainage happened in less than 6 months, with an apparent connection between three lakes spanning more than 130 km. Hydro-potential analysis of the glacier bed shows a large number of small closed basins that should trap water produced by subglacial melt, although the observed large-scale motion of water suggests that water can sometimes locally move against the apparent potential gradient, at least during lake-drainage events. This shows that there are important limitations in the ability of hydro-potential maps to predict subglacial water flow. An interpretation based on a map of the melt rate suggests that lake drainages of this type should take place every 20–80 years, depending on the connectivity of the water flow at the bed. Although we observed an acceleration in the downstream part of TWG immediately before the start of the lake drainage, there is no clear connection between the drainage and any speed change of the glacier.

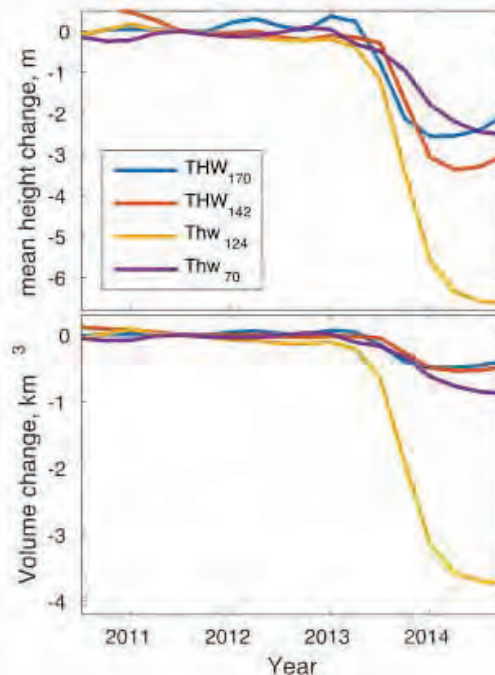
### 1 Background

The Amundsen Sea embayment is one of the fastest-changing part of Antarctica, with large changes since at least the 1990s (Rignot, 2008). Increased flow of Thwaites Glacier (TWG) is responsible for around half of the ice-sheet mass loss from this sector (Medley et al., 2014), in response

to these large changes. NSF's AGASEA and NASA's Ice-Bridge programmes have flown extensive surveys measuring ice thickness and bed elevation in this area, with the twin goals of measuring mass-balance changes and enabling accurate ice-flow modelling for the region. As a result, the bed of TWG has been mapped in detail, allowing mapping of basal shear stress and potential subglacial water-flow paths. These reveal abundant basal meltwater production, estimated at about  $3.5 \text{ km}^3 \text{ yr}^{-1}$  and averaging  $\sim 19 \text{ mm yr}^{-1}$  (Joughin et al., 2009). Melt production is concentrated in the fast-flowing lower trunk of the glacier but is locally larger than  $20 \text{ mm yr}^{-1}$  even in some regions within the slow-flowing catchment. Interpretation of radar-reflection properties has also led researchers (Schroeder et al., 2013, 2015) to identify an upstream region where water may drain through a persistent, distributed network of high-aspect-ratio canals and a downstream region drained by larger canals that concentrate water into a small area. The combination of radar observations and estimated melt rates led to a map of geothermal heat flux, based on the assumption that the basal water system was in equilibrium with steady-state melt rates (Schroeder et al., 2014). Further, the spatial correlation between relatively high driving stress in the lower trunk and the hypothesized channelized drainage system has led to speculation that the character of the basal water system plays a role in the stability of the glacier and that changes in this water system could lead to accelerated grounding-line retreat (Schroeder et al., 2013).

Active subglacial lakes (lakes that drain or fill over the course of a few years or less) have been identified throughout Antarctica (Smith et al., 2009). Well-documented lake sys-

# b-glacial lakes



Peak discharge of  $240 \text{ m}^3$  per second

Much of the drainage happened in less than 6 months, with an apparent connection between three lakes spanning more than 130 km.

### Drainage event in 2013

The centres of the features are approximately 70, 124, 142, and 170 km upstream of the grounding line

# Examples of results

High-resolution surface elevation change (2010 to 2016) from CryoSat shows channelized thinning (5 km-wide and 60 km-long) of the ice shelf in Antarctica. Thinning is related to channelized basal melting controlled by ocean circulation and cavity geometry.



ESA UNCLASSIFIED - For Official Use



Energy and Environment

## Worrying new research finds that the ocean is cutting through a key Antarctic ice shelf



Sign in

News

Sport

Weather

Shop

Earth

By Chris Mooney October 11

### NEWS

Home Video World UK Business Tech Science Stories Entertainment

Scientists have identified a way in which the effects of Antarctic melting can be enhanced.

Their new satellite observations of the Dotson Ice Shelf show its losses, far from being even, are actually focused on a long, narrow sector.

In places, this has cut an inverted canyon through more than half the thickness of the shelf structure.

If the melting continued unabated, it would break Dotson in 40-50 years, not the 200 years currently projected.

"That is unlikely to happen because the ice will respond in some way to the imbalance," said Noel Gourmelen, from the University of Edinburgh, UK.

"It's possible the area of thinning could widen or the flow of ice could change. Both would affect the rate at which the channel forms.

"But the important point here is that Dotson is not a flat slab and it can be much thinner in places than we think it is and much closer to a stage where it might experience major change."

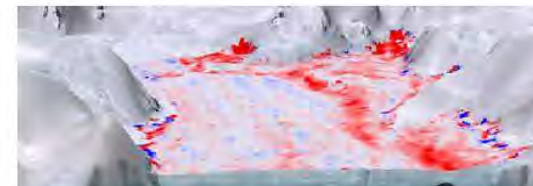
A new scientific study published into the underside of one of the enormous ice continent.

The Dotson ice shelf, which lies between 1,000 and 1,600 feet Noel Gourmelen, a researcher which was just published in G

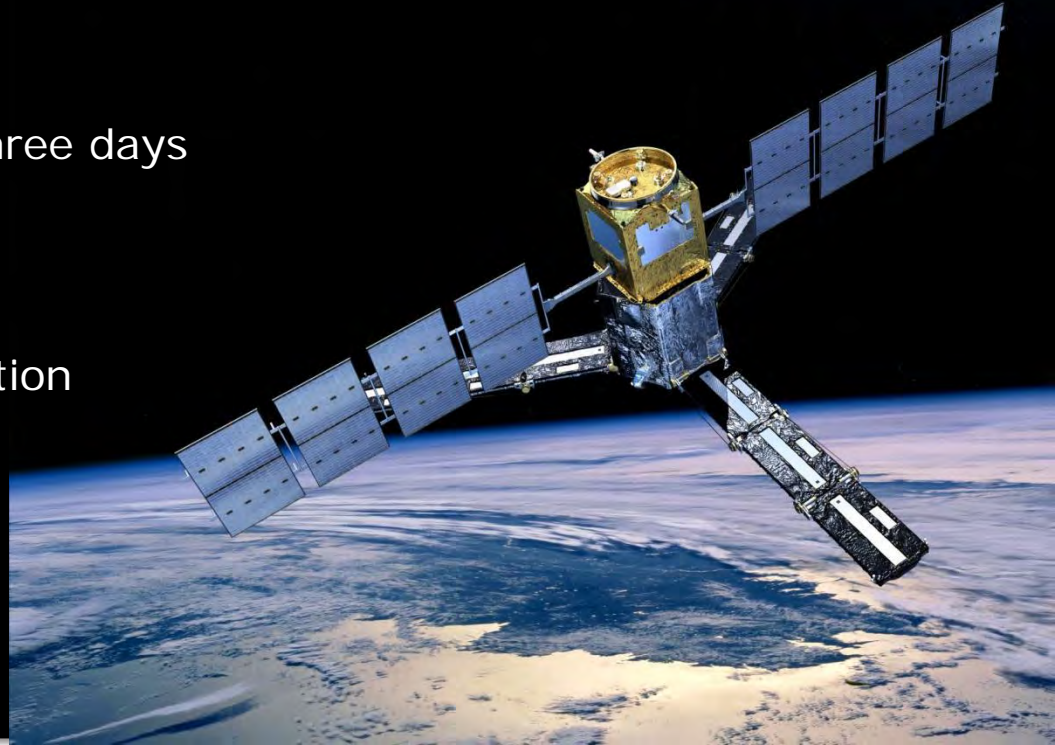
The reason is the same one that West Antarctica — warm ocean

- British mission to giant berg approved
- Giant iceberg splits from Antarctic
- Shells record Antarctic glacier retreat
- Satellite's ice vision is boosted

Energy and Environment newsletter



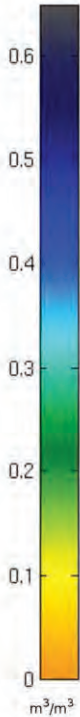
- Launched 02 November 2009
- Data delivery since February 2010
- Complete Earth coverage within three days
- Radio Frequency Interference (RFI) mitigation continues
- Outstanding international cooperation



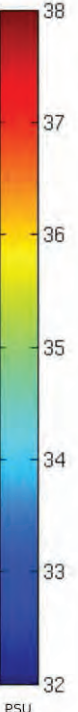
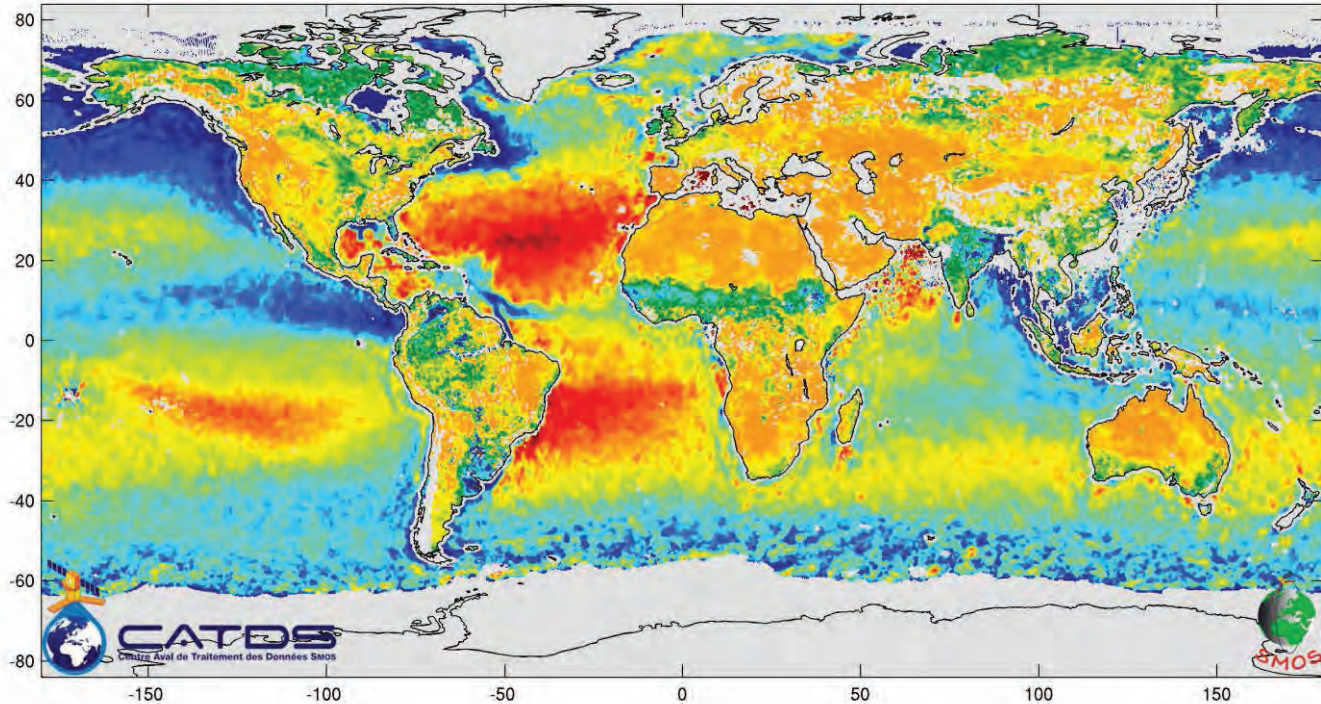
# SMOS Measurements



Aug 2015



SM



OS

ESA UNCLASSIFIED - For Official Use

08/03/2017 | Slide 38



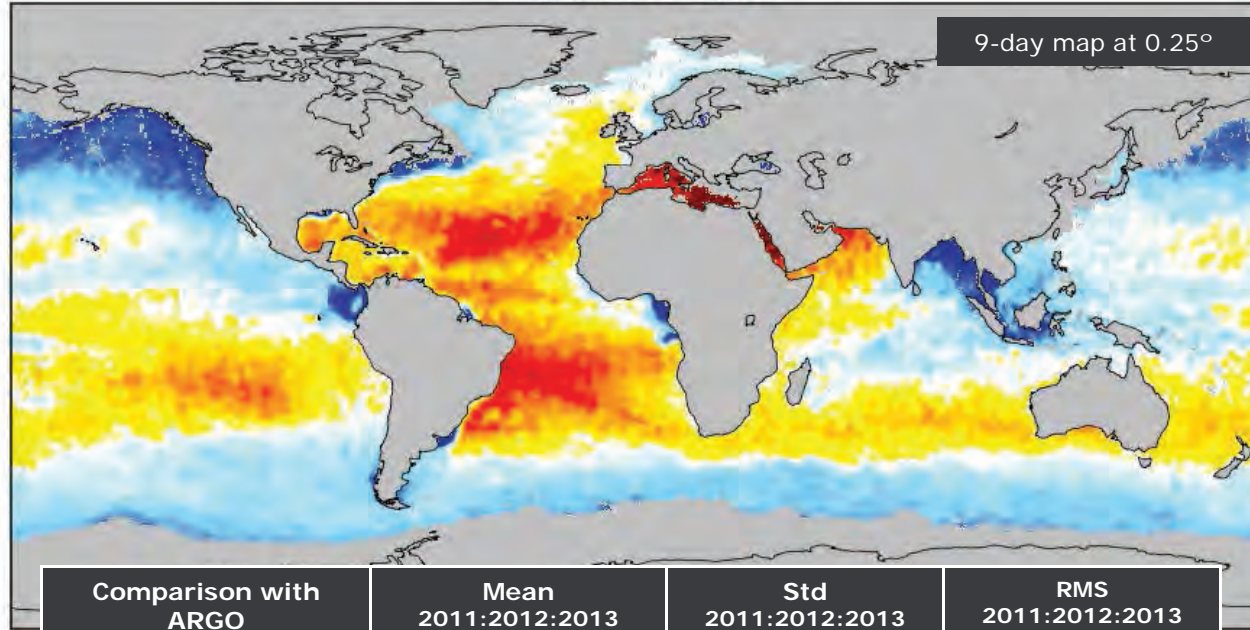
European Space Agency

# SMOS Sea Surface Salinity

Time: 2013-01-24 00:24:44



9-day map at 0.25°



SMOS provides SSS over open oceans .

Retrievals present several challenges over close seas.

New processing methods improve coverage: All the brightness temperatures are processed separately, empirically debiased with the corresponding SMOS-based climatology

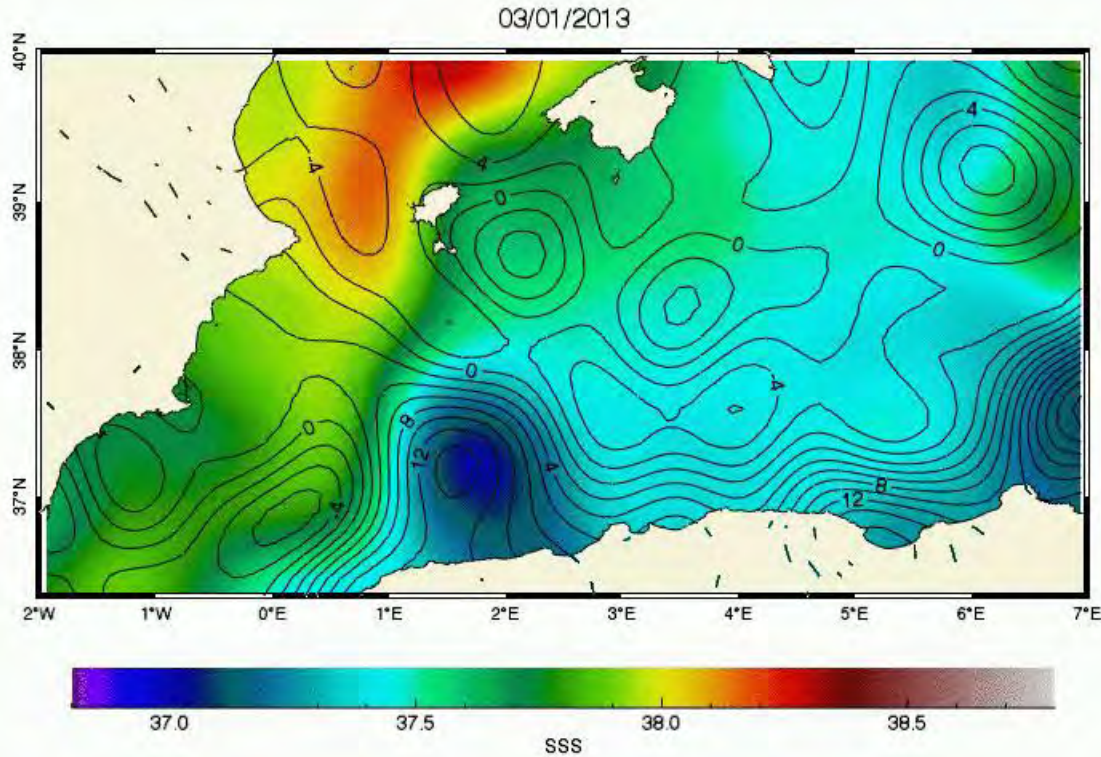
Comparison with ARGO	Mean 2011:2012:2013	Std 2011:2012:2013	RMS 2011:2012:2013
Global	0.01:0.01:0.00	0.31:0.31:0.31	0.31:0.31:0.31
Southern Ocean	-0.13:-0.12:-0.18	0.22:0.22:0.22	0.26:0.26:0.26
Equatorial Oceans	0.13:0.12:0.11	0.27:0.27:0.28	0.31:0.30:0.31
Mediterranean Sea	-0.16:-0.35:-0.27	0.25:0.37:0.32	0.32:0.52:0.44

*Olmedo et al., "Debiased non-Bayesian retrieval: A novel approach to SMOS Sea Surface Salinity", Remote Sensing of Environment 193,103-126 (2017)*

Source: Antonio Turiel, SMOS BEC



# New L4 SSS approach:



New techniques:

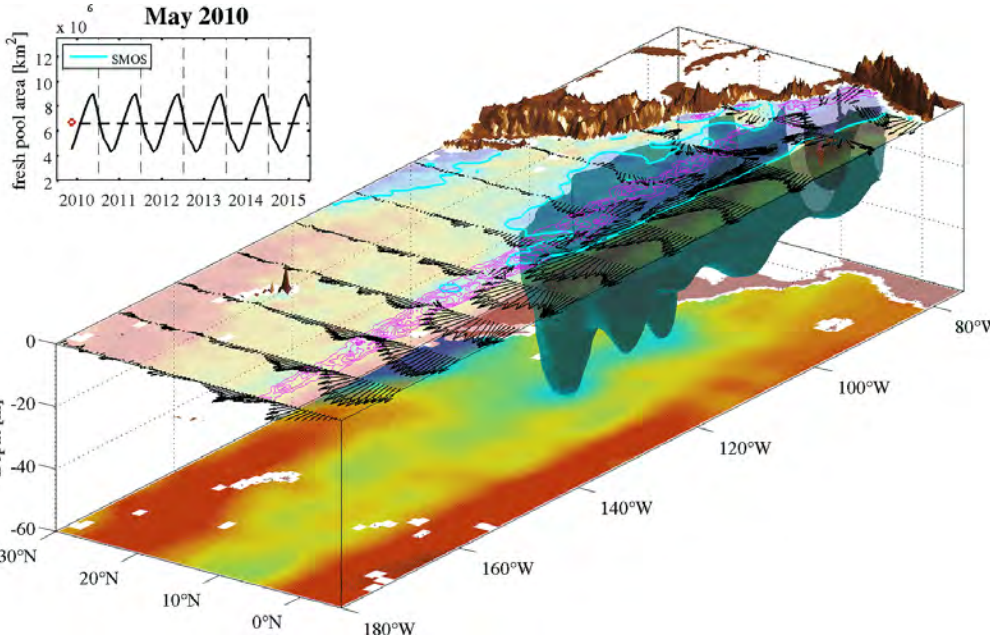
Combining SMOS L3 SS with SST observations may improve the spatial and temporal resolution of the SSS retrievals allowing the detection of eddies in the Algerian Basin.

*E. Olmedo, et. al, RSE, 2016*

*J. Isern-Fontanet et al., GRL, 2016*

Source: Antonio Turiel, SMOS BEC

# SMOS looking at ocean fresh water dynamics



ESA's SMOS satellite has found a rise in fresh water in the tropical Pacific Ocean during last year's El Niño event.

In the equatorial Pacific Ocean, surface waters have low salt concentration in the far east and far west boundaries of the basin owing to heavy rain. These areas are known as the Eastern and Western Pacific Fresh Pools.

Both pools move from east to west on a seasonal basis because of changes in the atmospheric forcing (such as heat, freshwater fluxes and wind speed) that affect rain, evaporation and currents.

The pools' position and extension are also subject to change on a longer time scale. One reason is El Niño, a warm phase of the ocean-atmosphere coupled phenomenon occurring every two to eight years.

Scientists have shown that low-salinity pools modify the ocean's vertical structure and change the impact of the atmospheric forcing on it.

Source: Sevastian , Ifremer, Living Planet Fellowship

ESA UNCLASSIFIED - For Official Use

08/03/2017 | Slide 41

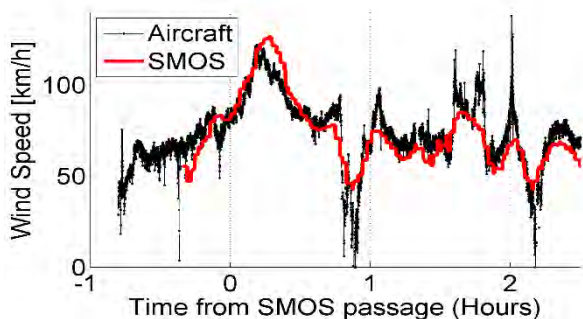


European Space Agency

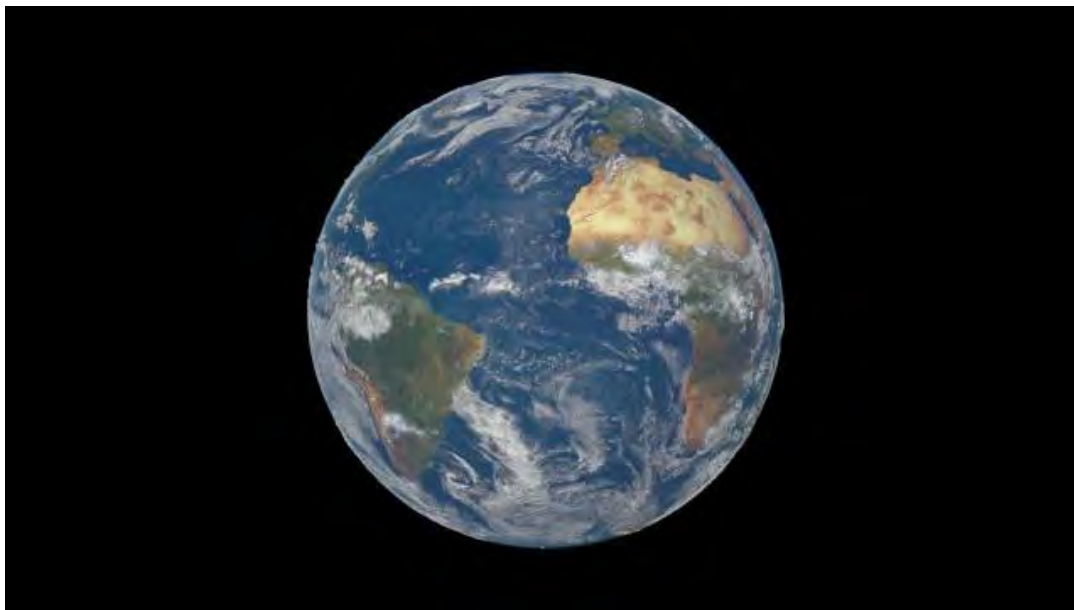
## SMOS for strong ocean wind retrieval

L-band is less sensitive to roughness and foam changes than at the higher C-band microwave frequencies. At the same time wind induced excess TB increases quasi-linearly with surface wind speed at a rate of  $0.3 \text{ K/m s}^{-1}$  and  $0.7 \text{ K/m s}^{-1}$  below and above the hurricane-force wind speed threshold ( $\sim 32 \text{ m s}^{-1}$ ).

SMOS wind measurements do not saturate over  $\sim 30 \text{ m/s}$  complementing scatterometer information that starts to fail at that wind speeds.



Surface wind speed during Hurricane Sandy taken from a NOAA aircraft and from SMOS (Credits: IFREMER/NOAA/HRD)



Sea Surface Wind Speed fields in meter per second retrieved from SMOS data over the Saffir-Simpson category 5 hurricane IGOR that developed in the North Atlantic ocean from 11 to 19 September 2010. (N.Reul (Ifremer) and J. Tenerelli (CLS)).

## SMOS explaining hurricanes behaviour over Amazone plume



**60 and 68% of hurricanes passing through the Amazon plume are category 4 and 5.**

**SMOS has shown how salinity in the surface waters change in the wake of a hurricane. This is the first time that such changes have been detected from space.**

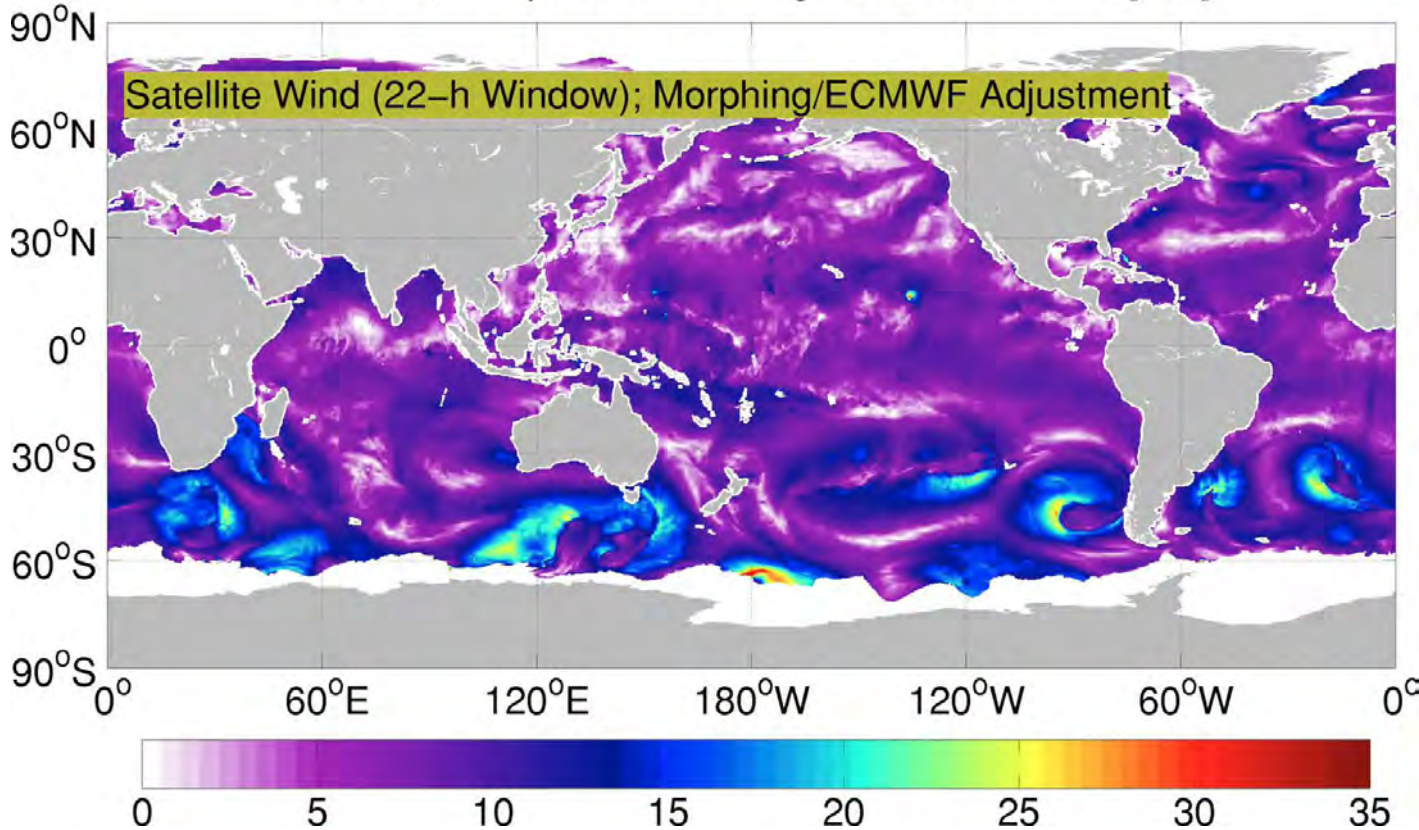
**Hurricane Igor caused the freshwater plume from the Amazon to mix with deeper saltier waters, increasing the salinity at the surface;**

**Fresh water from the plume creates a significant salinity-driven stratification that inhibits the SST cooling effect; hence the reduction of hurricane energy;**

**Salinity changes caused by Hurricane Igor. Approximately 1 GT of fresh water has been removed from the surface and mixed with deeper salty waters (Credits: IFREMER/CLS)**

# SMOS ocean winds: New multi-satellite blended product

## 10-m Wind Speed for 01-Aug-2015 00:00 UTC [m/s]



SMOS data has been proved to be a valid input to provide strong ocean wind speeds without saturation even over 35 m/s.

A new approach for combining non-synoptic satellite wind speeds (SMOS, SMAP and AMSR-2) to create synoptic wind maps is showed here that use variational data assimilation together with an atmospheric model (such as ECMWF).

**Source: IFREMER, OceanDataLab (FR)**



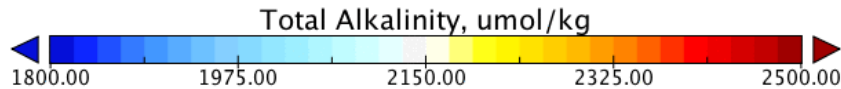
# First satellite based ocean acidification observations



Total alkalinity from SMOS (waters ability to resist a change in pH). The pulses of very low values are due to the large river outflow from the Amazon during the wet season.

**This is the first** EO-based synoptic view of Total alkalinity anywhere on Earth and it illustrates how the Amazon impacts much of the Central Atlantic.

This was only possible through using satellite Earth observation.



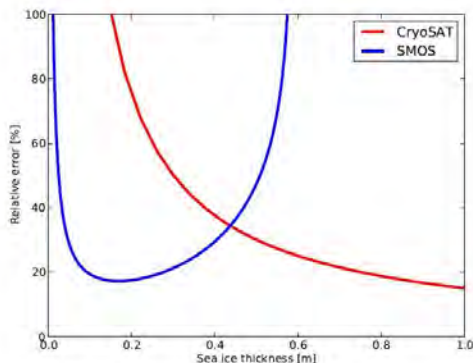
**Source: PML (UK)  
Pathfinder-OA**



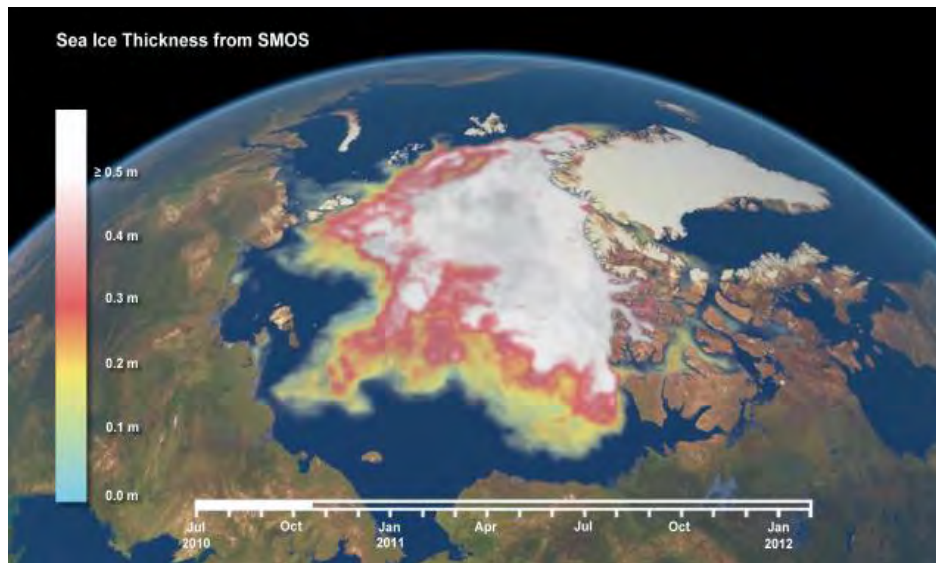
A novel algorithm and processor to derive estimates of the thin sea ice thickness up to 0.5m from SMOS Tbs has been developed and validated.

This is now transferred to operations: i.e., systematic generation of the product;

This new data complements Cryosat measurements with larger errors below 0.4m.

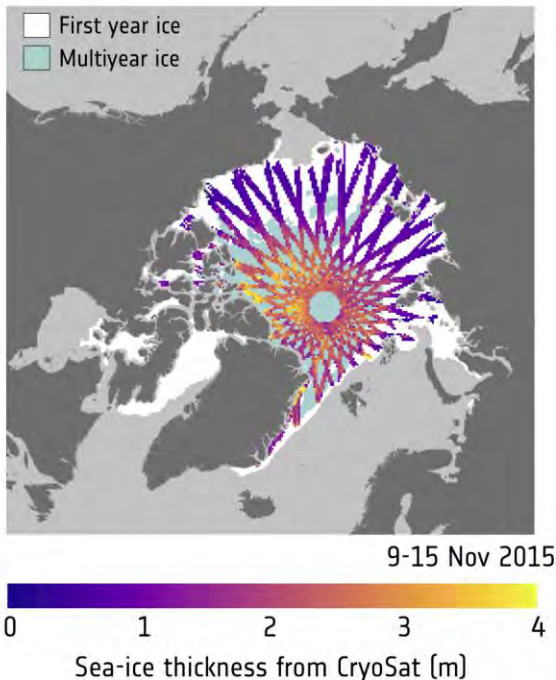


Relative error in sea ice thickness for both SMOS and Cryosat (Kaleschke et al., TCD, 2009)



Thin sea ice thickness derived from SMOS (<0.5) from July 2010 to January 2012. Credits: Lars Kaleschke, Xiangshan Tian-Kunze, Nina Maaß, KlimaCampus, University of Hamburg

# SMOS and Cryosat joining forces



University of Hamburg and the Alfred Wegener Institute (AWI) in Germany have developed a “full-range” sea ice product combining data for SMOS and CryoSat satellites;

While the accuracy of measurements from CryoSat increases with increasing ice thickness, SMOS data are more accurate when the sea ice is relatively thin, less than half a metre.

CryoSat measurements yield high-spatial resolution information and cover the Arctic every month. While SMOS offers daily images, they are a much coarser resolution than CryoSat.

Products have been merged to generate information on thin sea-ice going back to 2010.



## A Weekly Arctic Sea-Ice Thickness Data Record from merged CryoSat-2 and SMOS Satellite Data

Robert Ricker<sup>1,2</sup>, Stefan Hendricks<sup>1</sup>, Lars Kaleschke<sup>3</sup>, Xiangshan Tian-Kunze<sup>3</sup>, Jennifer King<sup>4</sup>, and Christian Haas<sup>1,5</sup>

<sup>1</sup>Alfred Wegener Institute, Helmholtz Centre for Polar and Marine Research, Bremerhaven, Bussestrasse 24, 27570 Bremerhaven, Germany

<sup>2</sup>Univ. Brest, CNRS, IRD, Ifremer, Laboratoire d’Océanographie Physique et Spatiale (LOPS), IUEM, 29280, Brest, France

<sup>3</sup>Institute of Oceanography, University of Hamburg, Bundesstrasse 53, 20146 Hamburg, Germany

<sup>4</sup>Norwegian Polar Institute, Tromsø, Norway

<sup>5</sup>York University, Toronto, Canada

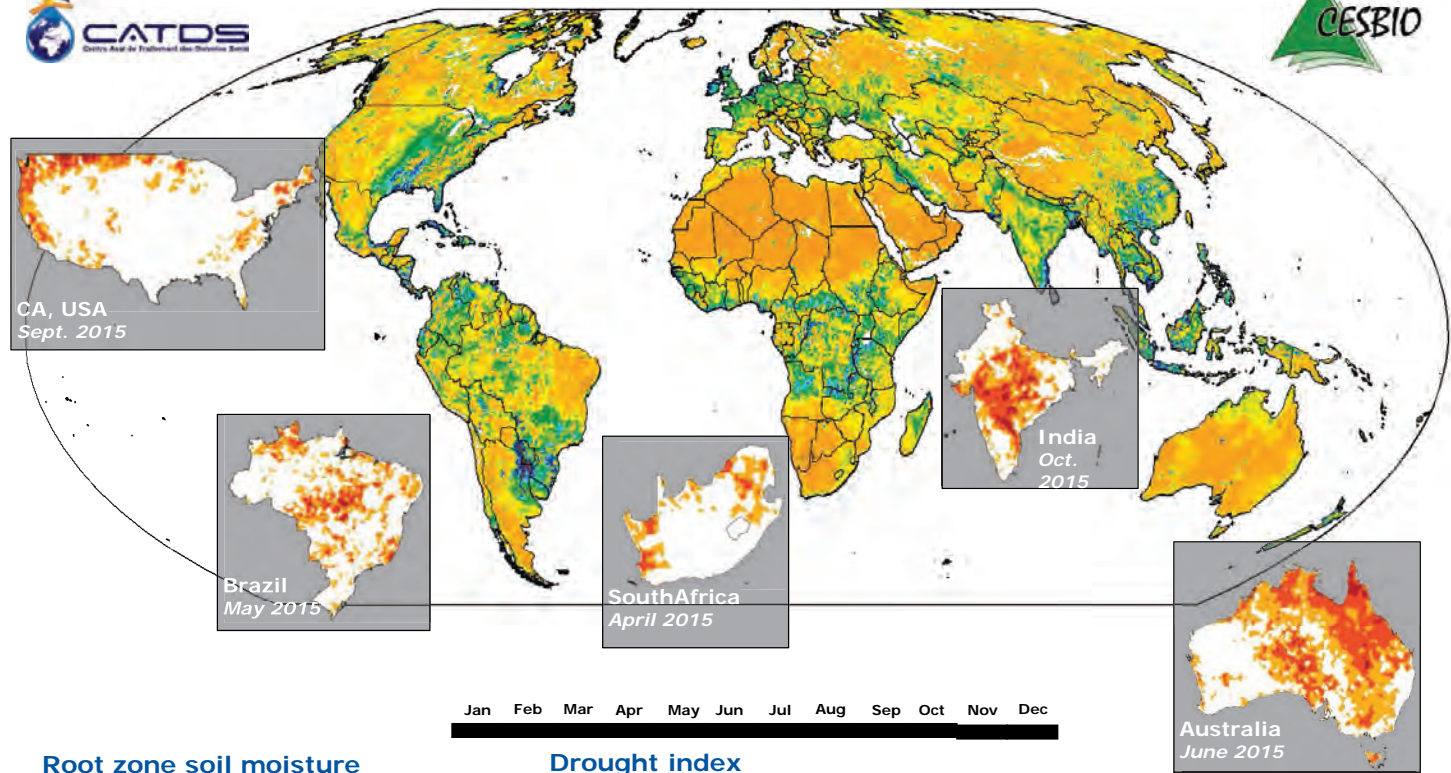
Correspondence to: Robert Ricker (Robert.Ricker@awi.de)

**Abstract.** Sea-ice thickness on global scale is derived from different satellite sensors using independent retrieval methods. Due to the sensor and orbit characteristics, such satellite retrievals differ in spatial and temporal resolution as well as in the sensitivity to certain sea-ice types and thickness ranges. Satellite altimeters, such as CryoSat-2 (CS2), sense the height of the ice surface above the sea level, which can be converted into sea-ice thickness. However, relative uncertainties associated with this method are large over thin ice regimes. Another retrieval strategy is realized by the evaluation of surface brightness temperature in L-Band microwave frequencies (1.4 GHz) with a thickness-dependent emission model, as measured by the Soil Moisture and Ocean Salinity (SMOS) satellite. While the radiometer based method loses sensitivity for thick sea ice (> 1m), relative uncertainties over thin ice are significantly smaller than for the altimetry-based retrievals. In addition, the SMOS product provides global sea-ice coverage on a daily basis unlike the narrow-swath altimeter data. This study presents the first merged product of complementary weekly Arctic sea-ice thickness data records from the CS2 altimeter and SMOS radiometer. We use two merging approaches: a weighted mean and an optimal interpolation scheme (OI). While the weighted mean leaves gaps between CS2 orbits, OI is used to produce weekly Arctic-wide sea-ice thickness fields. The benefit of the data merging is shown by a comparison with airborne electromagnetic induction sounding measurements. When compared to airborne thickness data in the Barents Sea, the merged products reveal a reduced root mean square deviation of about 0.7 m compared to the CS2 retrieval and therefore demonstrate the capability to enhance the CS2 retrieval in thin ice regimes.

### 1 Introduction

Sea ice is an essential climate variable and affects many climate related processes, such as heat transfer between ocean and atmosphere or ocean circulation, but also marine operations (Meier et al., 2014). For decades, the variability and changes of the ice covered region have been routinely observed by satellite remote sensing of sea-ice extent and area. However, the thickness of sea ice is a crucial parameter for the ice mass balance and is more difficult to observe. Recent satellite altimeter missions such as ICESat or CryoSat-2 (CS2) demonstrated the capability to provide Arctic sea-ice thickness and volume estimates

# SMOS monitoring major droughts in 2015



Root zone soil moisture



Drought index



[ahmad.albitar@cesbio.cnrs.fr](mailto:ahmad.albitar@cesbio.cnrs.fr)

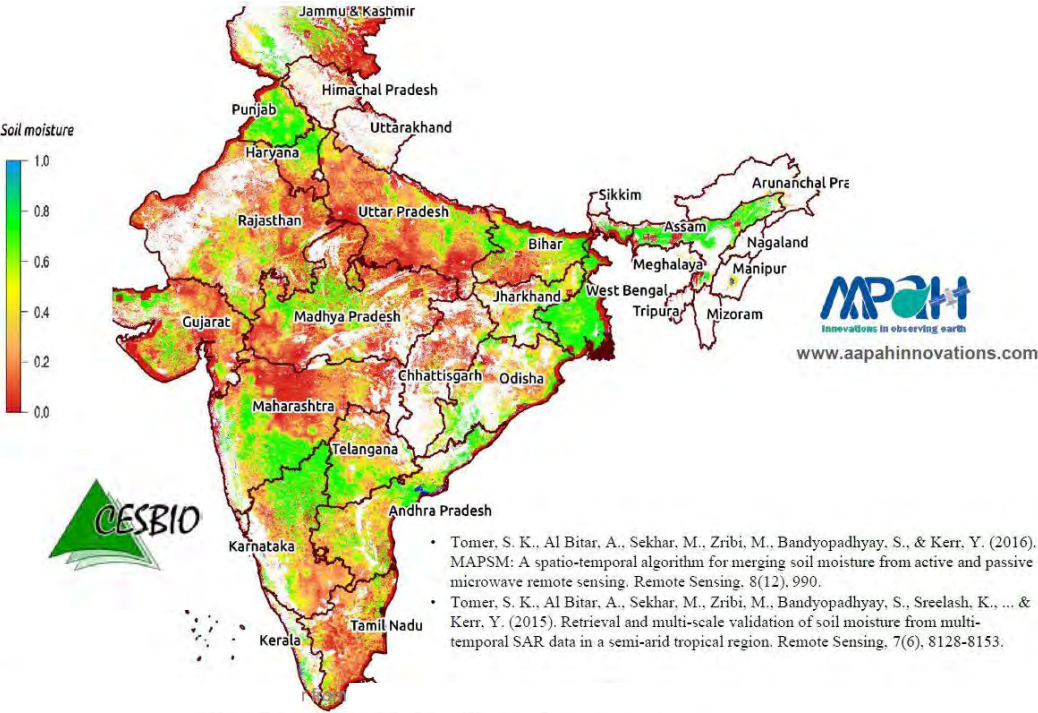
ESA UNCLASSIFIED - For Official Use

08/03/2017 | Slide 48

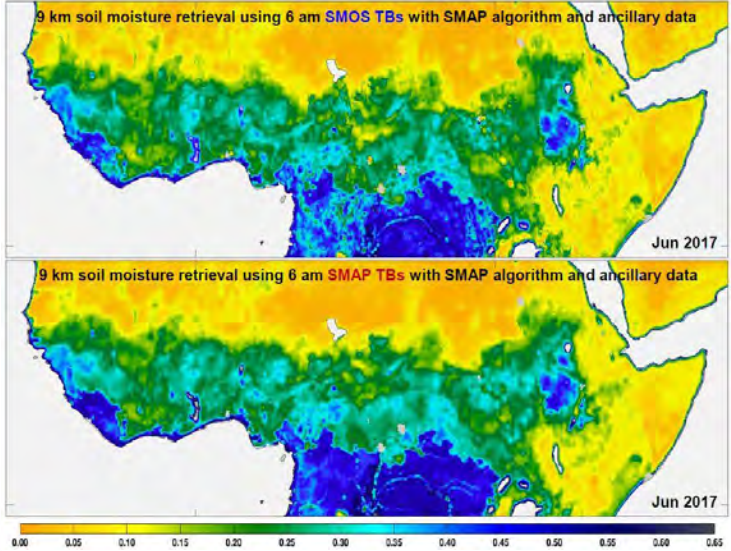


European Space Agency

# SMOS Developments



SMOS and S1 HR Soil Moisture  
500m. Source: CESBIO



Consistent SMOS and SMAP TBs, algorithm, and ancillary data lead to a new consistent SMOS/SMAP soil moisture product. Source: CESBIO/NASA;





## Correcting satellite-based precipitation products through SMOS soil moisture data assimilation in two land-surface models of different complexity: API and SURFEX

Carlos Román-Cascón<sup>a,\*</sup>, Thierry Pellarin<sup>a</sup>, François Gibon<sup>a</sup>, Luca Brocca<sup>c</sup>, Emmanuel Cosme<sup>a</sup>, Wade Crow<sup>d</sup>, Diego Fernández-Prieto<sup>a</sup>, Yann H. Kerr<sup>b</sup>, Christian Massari<sup>e</sup>

<sup>a</sup> Univ. Grenoble Alpes, CNRS, IRD, Grenoble INP, ECI, Grenoble F-38000, France

<sup>b</sup> Centre d'Etudes Spatiales de la Biosphère (CESBIO), Université Toulouse 3 CNRS CNRS IRD, Toulouse, France

<sup>c</sup> National Research Council CNR, Research Institute for Geo-Hydrological Protection, Perugia, Italy

<sup>d</sup> Hydrology and Remote Sensing Laboratory, USDA Agricultural Research Service, Beltsville, MD, USA

<sup>e</sup> European Space Agency (ESA), Frascati, Italy

### ARTICLE INFO

**Keywords:**  
Rainfall  
Soil moisture  
SMOS  
API  
SURFEX  
Particle filter

### ABSTRACT

Global rainfall information is useful for many applications. However, real-time versions of satellite-based rainfall products are known to contain errors. Recent studies have demonstrated how the information about rainfall intrinsically contained in soil moisture data can be utilised for improving rainfall estimates. That is, soil moisture dynamics are impacted for several days by the accumulated amount of rainfall following within a particular event. In this context, soil moisture data from the Soil Moisture Ocean Salinity (SMOS) satellite is used in this study to correct rainfall accumulation estimates provided by satellite-based real-time precipitation products such as CMORPH, TRMM-3B42RT or PERSIANN. An algorithm based on the SMOS measurements data assimilation is tested in two land-surface models of different complexity: a simple hydrological model (Antecedent Precipitation Index (API)) and a more sophisticated state-of-the-art land-surface model (SURFEX (Surface Externalisée)). We show how the assimilation technique, based on a particle filter method, generally leads to a significant improvement in rainfall estimates, with slightly better results for the simpler (and less computationally demanding) API model. This methodology has been evaluated for six years at ten sites around the world with different land use and climatological features. The results also show the limitations of the methodology in regions highly affected by mountainous terrain, forest or intense radio-frequency interference (RFI), which can notably affect the quality of the retrievals. The satisfactory results shown here invite the future operational application of the methodology in near-real time on a global scale.

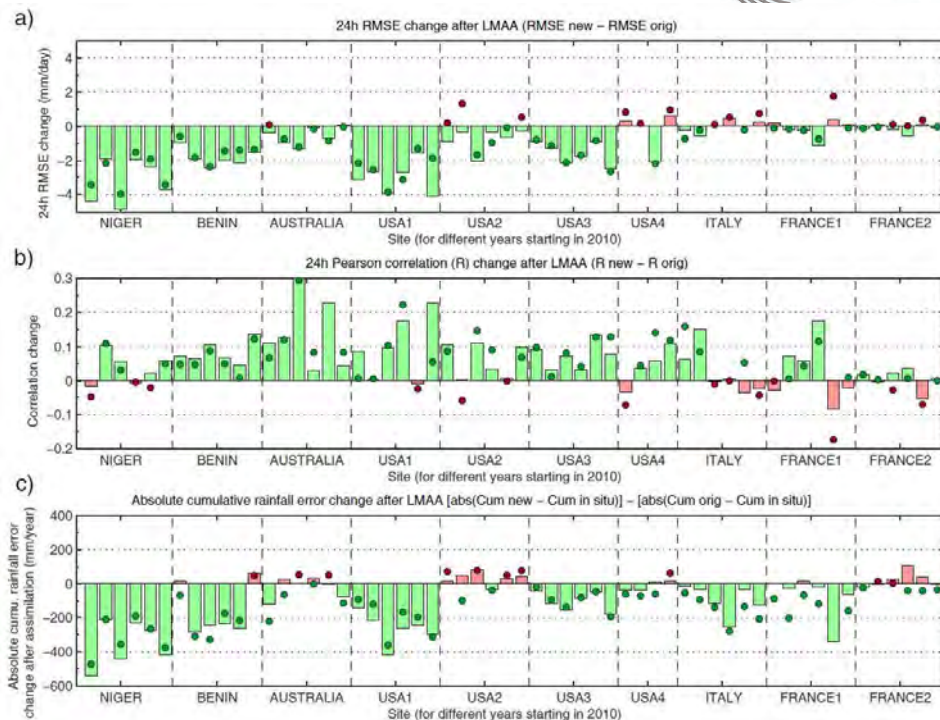
### 1. Introduction

Precipitation is a key variable of the water cycle, whose estimation is crucial for many applications (Brocca et al., 2016). Accurate estimates of the amount of water which reaches the ground at specific areas in near-real time are needed for hydrological applications, including flood (Wake, 2013; Jongman et al., 2014; Casse et al., 2015; Lievens et al., 2015) or landslide (Van Asch et al., 1999; Guzzetti et al., 2007; Iverson, 2000; Pennington et al., 2014) emergency response planning. Rainfall accumulation estimates are also very important for agricultural strategy and modelling (Fisher, 1925; French and Schultz, 1984; Alphonkpe et al., 2011; Ramarohetra et al., 2013). Besides, accurate precipitation data is certainly decisive for data assimilation in

numerical weather prediction models, since it highly affects surface energy fluxes that will drive the evolution of the planetary boundary layer (Pielke et al., 1998) which is linked to the formation of mesoscale and/or synoptic weather systems. Finally, the link between the spatio-temporal distribution of precipitation and the freshwater availability at several regions of the Earth is crucial for decision-making to mitigate extreme situations (Hou et al., 2014; Shannon et al., 2008), such as intense droughts.

Rain gauges provide the most accurate and reliable data to obtain the amount of rainfall at a point on the Earth's surface (Larza and Vuerich, 2009). However, the heterogeneous (temporal and spatial) characteristic of rainfall makes the use of the information provided by one (or a few) station(s) not sufficient to address the large-scale

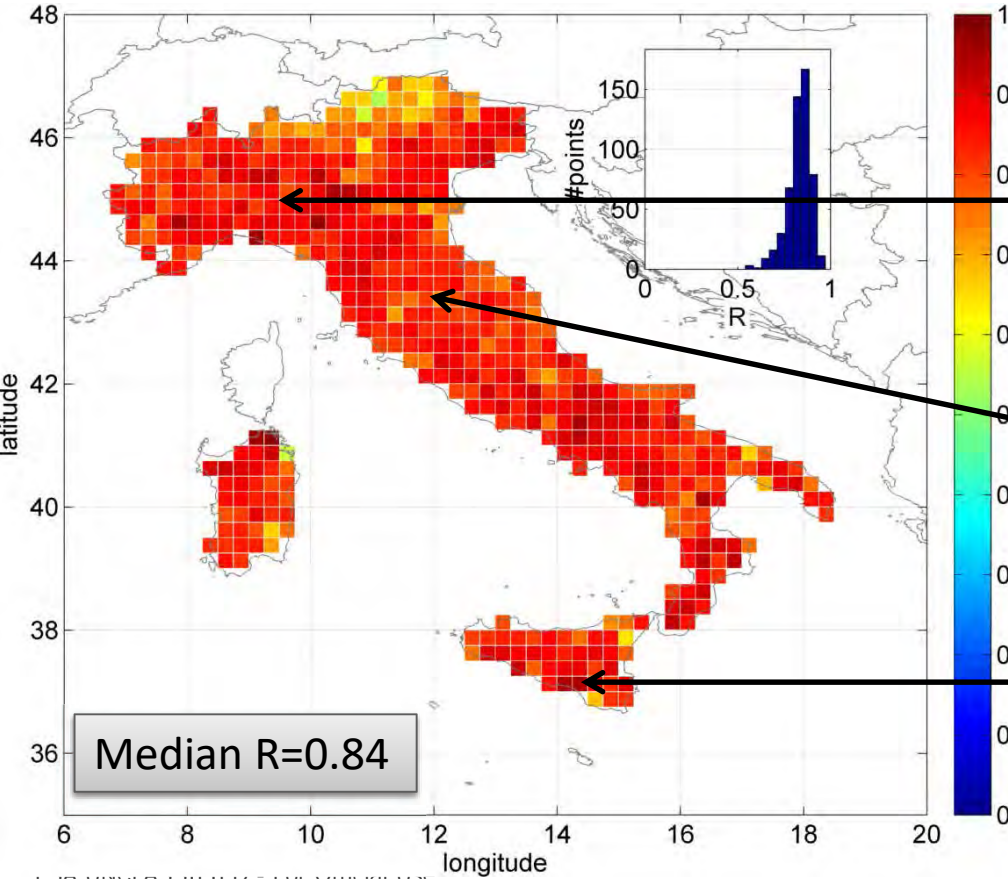
*d* (Gascon et al., 2017)



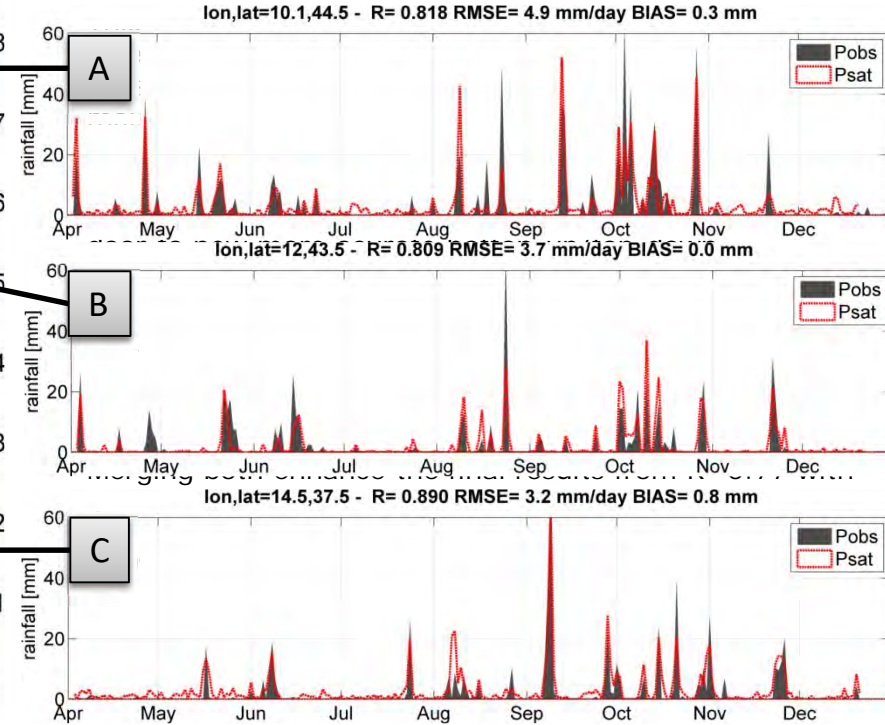
a) 24h RMSE change (mm/day). b) 24h Pearson correlation change. c) Absolute cumulative error change (mm/year). The results are shown for 10 sites (separated by vertical dashed lines) and for years from 2010 to 2015 (except USA 4, which is only from 2010 to 2013). Green colours indicate improvements and red ones worsenings regarding the performance scores of the original products;



# Estimating Rainfall from Soil Moisture



New methods to derive and improve traditional satellite rainfall products using soil moisture have been developed.



ESA UNCLASSIFIED - For Official Use



## How much water is used for irrigation? A new approach exploiting coarse resolution satellite soil moisture products

Luca Brocca<sup>a,\*</sup>, Angelica Tarpanelli<sup>b</sup>, Paolo Filippucci<sup>b</sup>, Wouter Dorigo<sup>c</sup>, Felix Zaussinger<sup>b</sup>, Alexander Gruber<sup>b,d</sup>, Diego Fernández-Prieto<sup>d</sup>

<sup>a</sup> Research Institute for Geo-Hydrological Protection, National Research Council, Perugia, Italy

<sup>b</sup> CLMARS – Research Group Climate and Environmental Remote Sensing, Department of Geodesy and Geoinformation, Vienna University of Technology, Vienna, Austria

<sup>c</sup> Department of Earth and Environmental Science, KU Leuven, Heverlee, Belgium

<sup>d</sup> European Space Agency, ESA-ESRIN, Brno, Italy

### ARTICLE INFO

#### Keywords:

Soil moisture  
Irrigation  
Remote sensing  
ASCAT  
SMAP  
SMOS  
AMSR2

### ABSTRACT

Knowledge of irrigation is essential for ensuring food and water security, and to cope with the scarcity of water resources, which is expected to exacerbate under the pressure of climate change and population increase. Even though irrigation is likely the most important direct human intervention in the hydrological cycle, we have only partial knowledge on the area of our planet in which irrigation takes place, and almost no information on the amount of water that is applied for irrigation.

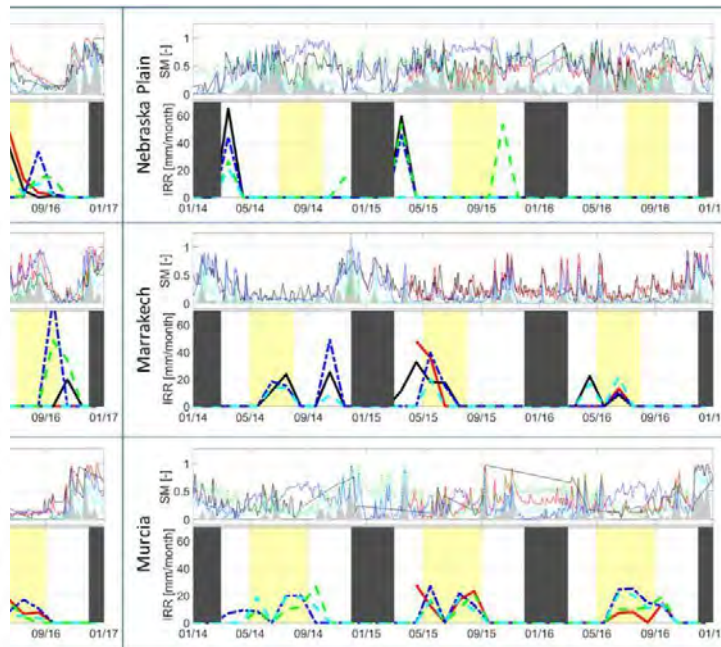
In this study, we developed a new approach exploiting satellite soil moisture observations for quantifying the amount of water applied for irrigation. Through the inversion of the soil water balance equation, and by using satellite soil moisture products as input, the amount of water entering into the soil, and hence irrigation, is determined. Through synthetic experiments, we first assessed the impact of soil moisture measurement uncertainty and temporal resolution, also as a function of climate, on the accuracy of the method. Second, we applied the proposed approach to currently available coarse resolution satellite soil moisture products retrieved from the Soil Moisture Active and Passive mission (SMAP), the Soil Moisture and Ocean Salinity (SMOS) mission, the Advanced SCATterometer (ASCAT), and the Advanced Microwave Scanning Radiometer 2 (AMSR-2). Nine pilot sites in Europe, USA, Australia and Africa were used as case study to test the method in a real-world application.

The synthetic experiment showed that the method is able to quantify irrigation, with satisfactory performance from satellite data with retrieval errors lower than  $-0.04 \text{ m}^3/\text{m}^3$  and revisit times shorter than 3 days. In the case studies based on real satellite data, qualitative assessments (due to missing in situ irrigation observations) showed that over regions in which satellite soil moisture products perform well, and which are characterized by prolonged periods without rainfall, the method shows good results in quantifying irrigation. However, at sites in which rainfall is sustained throughout the year, the proposed method fails in obtaining reliable performances. Similarly, low performances are obtained in areas where satellite products uncertainties are too large, or their spatial resolution is too coarse with respect to the size of the irrigated fields.

### 1. Introduction

It is estimated that over 70% of global freshwater is consumed by irrigation (FAO, 2006; Foley et al., 2011). Irrigated land comprises 1/5 of the world's cultivated area and supplies 2/5 of the world's food (Droogers et al., 2010). Climate change and population growth are expected to further increase the irrigation demand pushing more pressure on available freshwater for food production, and many areas which already experience water scarcity (Vörösmarty et al., 2000;

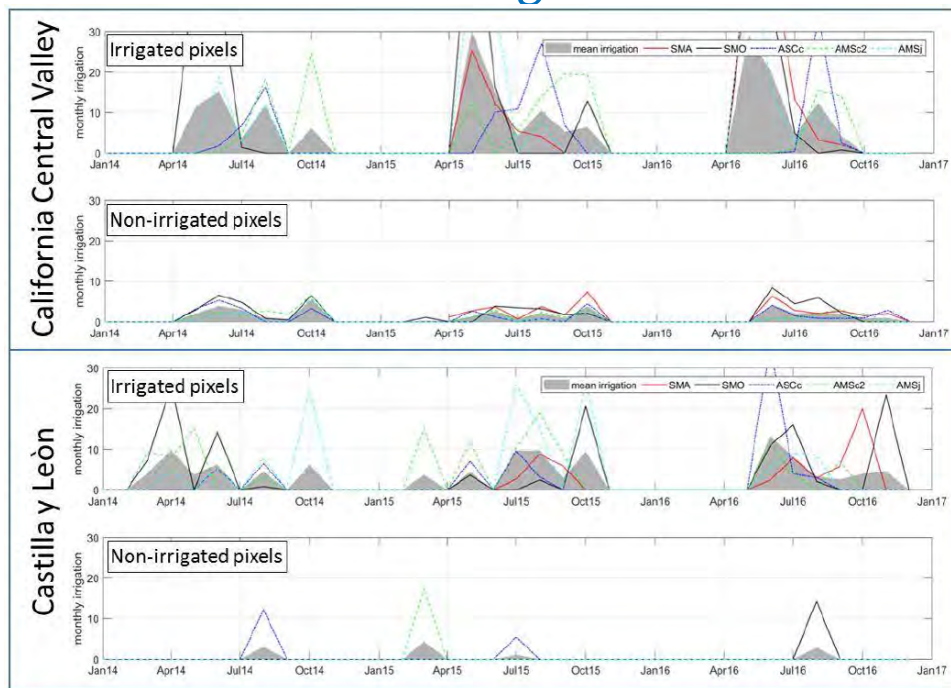
Röckström et al., 2012; Kummu et al., 2016). Therefore, quantitative knowledge on resources used for irrigation is essential for stakeholders and companies involved in the management of agricultural services and food production that need accurate and timely information for ensuring food and water security (Delnes et al., 2017). Additionally, information on irrigation is needed in many research applications e.g., for the assessment of the anthropogenic impact on the water and energy cycle (Bonfils and Lobell, 2007; Wada et al., 2014), to study the water budget closure in large scale hydrological and climate modelling (Döll and



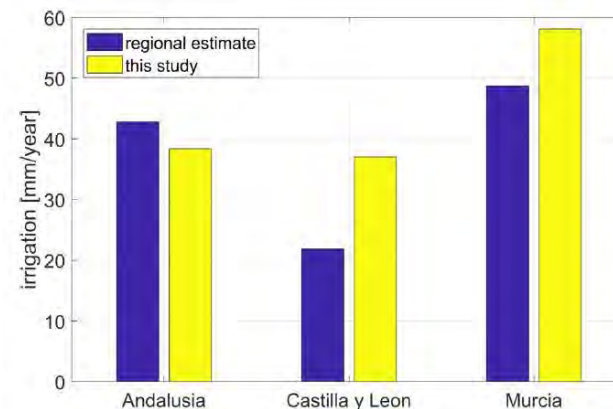
*n quantification for few pilot sites. Each panel shows on the top the satellite observed normalized rainfall (weekly), the bottom panel shows the estimated soil moisture product. Thin lines are estimated irrigation signals that are not allowed areas are the periods in which irrigation typically occur*

\* Corresponding author at Research Institute for Geo-Hydrological Protection, National Research Council, Via della Madonna Alta 126, 06128 Perugia, Italy.  
E-mail address: [luca.brocca@rpi.cnr.it](mailto:luca.brocca@rpi.cnr.it) (L. Brocca).

# Can EO estimate irrigation?



*comparison between monthly irrigation estimates for irrigated and non-irrigated pixels for California Central Valley and Castilla y León. The grey area represents the average irrigation obtained with the different products*



*Comparison of average annual irrigation values obtained from statistical surveys (Instituto Nacional de Estadística) and estimated in this study for the three pilot sites in Spain.*

## Satellite passive microwaves reveal recent climate-induced carbon losses in African drylands

Martin Brandt<sup>1,2\*</sup>, Jean-Pierre Wigneron<sup>3,4\*</sup>, Jerome Chave<sup>1</sup>, Torbern Tagesson<sup>1</sup>, Josep Peñuelas<sup>5,6,7</sup>, Philippe Clais<sup>8</sup>, Kjeld Rasmussen<sup>9</sup>, Feng Tian<sup>10</sup>, Cheikh Mbow<sup>11</sup>, Amen Al-Yaari<sup>12</sup>, Nemesio Rodriguez-Fernandez<sup>13</sup>, Guy Schurgers<sup>14</sup>, Wenmin Zhang<sup>15</sup>, Jinfeng Chang<sup>16</sup>, Yann Kerr<sup>17</sup>, Alexandre Verger<sup>18</sup>, Compton Tucker<sup>19</sup>, Arnaud Mialon<sup>1</sup>, Laura Vang Rasmussen<sup>1</sup>, Lei Fan<sup>20</sup> and Rasmus Fensholt<sup>1</sup>

The African continent is facing one of the driest periods in the past three decades as well as continued deforestation. These disturbances threaten vegetation carbon (C) stocks and highlight the need for improved capabilities of monitoring large-scale aboveground carbon stock dynamics. Here we use a satellite dataset based on vegetation optical depth derived from low-frequency passive microwaves (L-VOD) to quantify annual aboveground biomass-carbon changes in sub-Saharan Africa between 2010 and 2016. L-VOD is shown not to saturate over densely vegetated areas. The overall net change in drylands (53% of the land area) was  $-0.05$  petagrams of C per year ( $\text{Pg C yr}^{-1}$ ) associated with drying trends, and a net change of  $-0.02$   $\text{Pg C yr}^{-1}$  was observed in humid areas. These trends reflect a high inter-annual variability with a very dry year in 2015 (net change,  $-0.67$   $\text{Pg C yr}^{-1}$ ) with about half of the gross losses occurring in drylands. This study demonstrates, first, the applicability of L-VOD to monitor the dynamics of carbon loss and gain due to weather variations, and second, the importance of the highly dynamic and vulnerable carbon pool of dryland savannas for the global carbon balance, despite the relatively low carbon stock per unit area.

The forests and savannas of Africa have attracted particular attention, because both climate change and land use pressure have large impacts on the carbon stocks of woody vegetation with immediate consequences for the global carbon balance<sup>1–3</sup>. Deforestation is a well-known threat not only to rainforests<sup>4–6</sup>, but also to savannah vegetation, which is also threatened by climatic extremes such as dry years<sup>7</sup>. However, the net balance of carbon stocks in the savannah vegetation, changes in plant growth rates (negatively impacted by humans and dry periods but positively affected by elevated  $\text{CO}_2$  levels)<sup>8</sup> and altered mortality of the woody vegetation are currently unknown<sup>9,10</sup>. We also do not know whether semi-arid regions in Africa, which were identified as an important carbon sink with a peak in the year 2011<sup>11</sup>, have become a carbon source following the recent extreme El Niño in 2015–2016<sup>12</sup>. Knowledge of the amount, distribution and turnover of carbon in African vegetation is crucial for understanding the effects of human pressure and climate change, but the shortcomings of optical and radar satellite products and the lack of systematic field inventories have led to considerable uncertainty in documenting patterns of carbon stocks, and their long-term change over the African continent<sup>13</sup>. Static carbon maps have been developed based on field plots and satellite data using light detection and ranging (LIDAR) and interferometric synthetic aperture radar backscattering observations<sup>14,15</sup>. These maps constitute the best benchmarks to date for carbon stored in living woody vegetation<sup>16,17</sup>. The application of different techniques, however, complicates the direct comparison of these maps,

and results differ in magnitude and spatial patterns<sup>18,19</sup>. Importantly, the temporal dynamics of carbon stocks cannot be derived from the above benchmark maps, impeding timely, repeated and reliable carbon assessments<sup>20</sup>. In contrast, the vegetation optical depth (VOD) derived from high frequency (1.5 GHz) passive microwave-based satellite systems has been used to monitor changes in vegetation carbon<sup>21,22</sup>. Although the coarse spatial resolution of passive microwaves (100 km gridded) has limited their application in the detection of the spatial heterogeneity of carbon stocks, this technology is an attractive alternative to other remote sensing systems, because microwaves at frequencies lower than 15 GHz are almost insensitive to atmospheric and cloud effects. However, high frequency VOD satellites over forested areas and is generally not considered to be an accurate tool for carbon monitoring<sup>23</sup>. The Soil Moisture and Ocean Salinity (SMOS) mission launched in 2009 was the first passive microwave-based satellite system operating at L-Band (1.4 GHz) frequency<sup>24</sup>. These low frequencies allow the satellite to sense deeper within the canopy layer with less influence of green non-woody plant components. The VOD derived from SMOS, hereafter L-VOD, is thus less sensitive to saturation effects<sup>25</sup>, marking an important step forward in the monitoring of carbon as a natural resource. In this study we use L-VOD to quantify the inter-annual dynamics of aboveground biomass stocks for the period 2010–2016. This study does not attempt at improving current aboveground carbon stock maps nor at a comparison with state-of-the-art data and maps on carbon stocks<sup>26,27</sup>.



## The high sensitivity of SMOS L-Band vegetation optical depth to biomass

Nemesio J. Rodriguez-Fernandez<sup>1</sup>, Arnaud Mialon<sup>1</sup>, Stephane Mermoz<sup>1</sup>, Alexandre Bouvet<sup>1</sup>, Philippe Richaume<sup>1</sup>, Ahmad Al Bitar<sup>1</sup>, Amen Al-Yaari<sup>1</sup>, Martin Brandt<sup>1</sup>, Thomas Kaminski<sup>1</sup>, Thy Le Toan<sup>1</sup>, Yann H. Kerr<sup>1</sup>, and Jean-Pierre Wigneron<sup>2</sup>

<sup>1</sup>Centre d'Etudes Spatiales de la Biosphère (CESBIO), Centre National d'Etudes Spatiales (CNES), Centre National de la Recherche Scientifique (CNRS), Institut de Recherche pour le Développement (IRD), Université Paul Sabatier, Université de Toulouse, 18 av. Edouard Belin, bpi 2801, 31401 Toulouse, France

<sup>2</sup>Interactions Sol-Plante-Atmosphère (ISPA), Unité Mixte de Recherche 1391, Institut National de la Recherche Agronomique (INRA), CS 20052, 33882 Villenave d'Ornon cedex, France

<sup>3</sup>Department of Geosciences and Natural Resources Management, University of Copenhagen, 1350 Copenhagen, Denmark

<sup>4</sup>The incision Lab, Hamburg, Germany

Correspondence to: N.J. Rodriguez-Fernandez (nemesio.rodriguez-fernandez@univ-ils3.fr)

**Abstract.** The vegetation optical depth (VOD) measured at microwave frequencies is related to the vegetation water content and provides information complementary to visible/infrared-vegetation indices. This study is devoted to the characterization of a new VOD data set obtained from SMOS (Soil Moisture and Ocean Salinity) satellite observations at L-band (1.4 GHz). Three different SMOS L-band VOD (L-VOD) data sets (SMOS Level 2, Level 3 and SMOS-IC) were compared with data sets on tree height, visible/infrared indices (NDVI, EVI), cumulated precipitation, and above ground biomass (AGB) for the African continent. For all relationships, SMOS-IC showed the lowest dispersion and highest correlation. Overall, we found a strong ( $R > 0.85$ ) correlation with no clear sign of saturation between L-VOD and four AGB data sets. The relationship linking L-VOD and tree height ( $R = 0.87$ ) and Rascini's AGB ( $R = 0.94$ ) was strong and linear. The relationships between L-VOD and three other AGB data sets were linear per land cover class, but with a changing slope depending on the land cover type. For low vegetation classes, the annual mean of L-VOD spans a range: from 0 to 0.7 and it is linearly correlated with the amount of the average annual precipitations. SMOS L-VOD showed a higher sensitivity to AGB as compared to NDVI and KVV-C-VOD (VOD measured, respectively, at 19, 10.7, and 6.9 GHz). The results showed that although the spatial resolution of L-VOD is coarse ( $\sim 100$  km), the high temporal frequency and sensitivity to AGB makes SMOS L-VOD a very promising index for large scale monitoring of the vegetation status, in particular biomass.

### 1 Introduction

Large scale monitoring of vegetation properties is crucial to understand water, carbon and energy cycles. The Normalized Difference Vegetation Index (NDVI, Tucker, 1979) computed from space-borne observations at visible and infrared wavelengths has been widely used since the 1980s to study vegetation changes and its implications on animal ecology (Pettenilli et al., 2005, 2011), global fire emissions (Van der Werf et al., 2010), deforestation and urban development (Esau et al., 2016), global

## Coupling of ecosystem-scale plant water storage and leaf phenology observed by satellite

Feng Tian<sup>1,2\*</sup>, Jean-Pierre Wigneron<sup>3\*</sup>, Philippe Clais<sup>4</sup>, Jérôme Chave<sup>5</sup>, Jérôme Ogée<sup>6</sup>, Josep Peñuelas<sup>7,8</sup>, Anders Rabild<sup>9</sup>, Jean-Christophe Domec<sup>9</sup>, Xiaoye Tong<sup>9</sup>, Martin Brandt<sup>10</sup>, Arnaud Mialon<sup>11</sup>, Nemesio Rodriguez-Fernandez<sup>12</sup>, Torbern Tagesson<sup>13</sup>, Amen Al-Yaari<sup>14</sup>, Yann Kerr<sup>15</sup>, Chi Chen<sup>16</sup>, Ranga B. Myneni<sup>16</sup>, Wenmin Zhang<sup>17</sup>, Jonas Ardo<sup>18</sup> and Rasmus Fensholt<sup>19</sup>

Plant water storage is fundamental to the functioning of terrestrial ecosystems by participating in plant metabolism, nutrient and sugar transport, and maintenance of the integrity of the hydraulic system of the plant. However, a global view of the size and dynamics of the water pools stored in plant tissues is still lacking. Here, we report global patterns of seasonal variations in ecosystem-scale plant water storage and their relationship with leaf phenology, based on space-borne measurements of L-band vegetation optical depth. We find that seasonal variations in plant water storage are highly synchronous with leaf phenology for the boreal and temperate forests, but asynchronous for the tropical woodlands, where the seasonal development of plant water storage lags behind leaf area by up to 180 days. Contrasting patterns of the time lag between plant water storage and terrestrial groundwater storage are also evident in these ecosystems. A comparison of the water cycle components in seasonally dry tropical woodlands highlights the buffering effect of plant water storage on the seasonal dynamics of water supply and demand. Our results offer insights into ecosystem-scale plant water relations globally and provide a basis for an improved parameterization of eco-hydrological and Earth system models.

Water stored in plant tissues participates in physiological and biochemical processes (for example, metabolism and nutrient/sugar transport) and sustains the integrity of the plant hydraulic system by buffering the imbalance between transpiration water loss and root-soil water uptake<sup>1–3</sup>. Water movement in plants is a passive process, following a gradient of water potential (from higher to lower) generated by transpiration demand (regulated by stomata)<sup>4</sup> and root-regulated water uptake<sup>5,6</sup>. Since 2010, in response to changes in environmental conditions and metabolic activities, plant water storage varies from diurnal to seasonal timescales as a function of plant structure and hydraulic strategies<sup>7</sup>. Studies on the dynamics of plant water storage typically use measurements of sap flow reversals and leaf water potential on individual trees over relatively limited periods<sup>8,9</sup>. Scaling up tree-level data to the ecosystem scale is challenging due to the high spatial heterogeneity of plant composition and soil properties, thus precluding large-scale (continental or global) estimates of the dynamics of plant water storage.

Satellite passive microwave radiometers sense the natural Earth surface thermal emission at wavelengths of 0.1–30 cm from both the soil and vegetation layers, quantified as brightness temperature. The vegetation layer is semi-transparent, allowing the microwave radiations passing through, and creating a vegetation optical depth (VOD) proportionally linked to the vegetation water content ( $\text{kg m}^{-2}$ )<sup>10</sup>. The higher the microwave frequency, the stronger the vegetation attenuation effect. The low-frequency L-band (1.4 GHz) VOD (L-VOD) can detect changes in plant

water storage even for dense forest canopies<sup>11–16</sup>, where the woody tissues of stems and branches hold most plant water<sup>17</sup>. This detection is not possible with VOD products at higher frequencies (>6 GHz), because their signals are dominated by the water status of canopy leaves<sup>18,19</sup>. Satellite-based VOD retrievals from X-Band (10.7 GHz) observations over the day and night have recently been used to map ecosystem-scale anisotropy—an indicator of stomatal regulation and water uptake<sup>20,21</sup>. Since 2010, the first satellite-based L-band radiometer carried by the Soil Moisture and Ocean Salinity (SMOS) mission<sup>22</sup> further has enabled global-scale monitoring of the dynamics in plant capacity water storage, which is another key functional trait in forest eco-hydrological processes.

Here, we used the SMOS L-VOD products<sup>23,24</sup> as a proxy for time and space variations in ecosystem-scale plant water storage, and examined its seasonal dynamics globally over the period 2011–2016. Since leaf area sence the transpiration flux and photosynthetic productivity, we also examined the coupling between seasonal variations in L-VOD and leaf phenology (defined as the seasonality of the satellite-observed leaf area index (LAI)).

### Results and discussion

**Seasonal amplitude of L-VOD.** We analysed the seasonal dynamics of ecosystem-scale plant water storage by concatenating six-year (2011–2016) SMOS L-VOD data into a mean yearly daily time series at a spatial resolution of 0.25° (Methods and Supplementary Fig. 1). Large land regions had substantial data gaps due to the influence of

<sup>1</sup>Department of Geosciences and Natural Resources Management, University of Copenhagen, Copenhagen, Denmark. <sup>2</sup>INRA, UMR 1091, INRA Nouvelles Acquisitions, Bordeaux Villenave d'Ornon, France. <sup>3</sup>Laboratoire Evolution et Diversité Biologique, Bâtiment 403 Université Paul Sabatier, Toulouse, France. <sup>4</sup>CNRS, Global Ecology Unit CSEAF-CSE-UIAR, Balatona, Spain. <sup>5</sup>CEAF, Cantanaya del Valle, Spain. <sup>6</sup>Laboratoire des Sciences du Climat et de l'Environnement, CEA-CNRS-UVSQ, CE Saclay des Marais, Gif sur Yvette, France. <sup>7</sup>CEAF, International Institute of Agrobiological Sciences, Tsukuba, Ibaraki, Japan. <sup>8</sup>Global Ecology Unit CSEAF-CSE-UIAR, Balatona, Spain. <sup>9</sup>CEAF, Cantanaya del Valle, Spain. <sup>10</sup>Bordeaux Sciences Agro, UMR 1391 INRA-ISA, Gradignan, France. <sup>11</sup>CESBIO, Université de Toulouse, CNRS/IRD/UPS, Toulouse, France. <sup>12</sup>Department of Earth and Environment, Boston University, Boston, MA, USA. \*e-mail: flian2012@gmail.com; jean-pierre.wigneron@inra.fr

# Swarm: ESA's Magnetic Field Mission

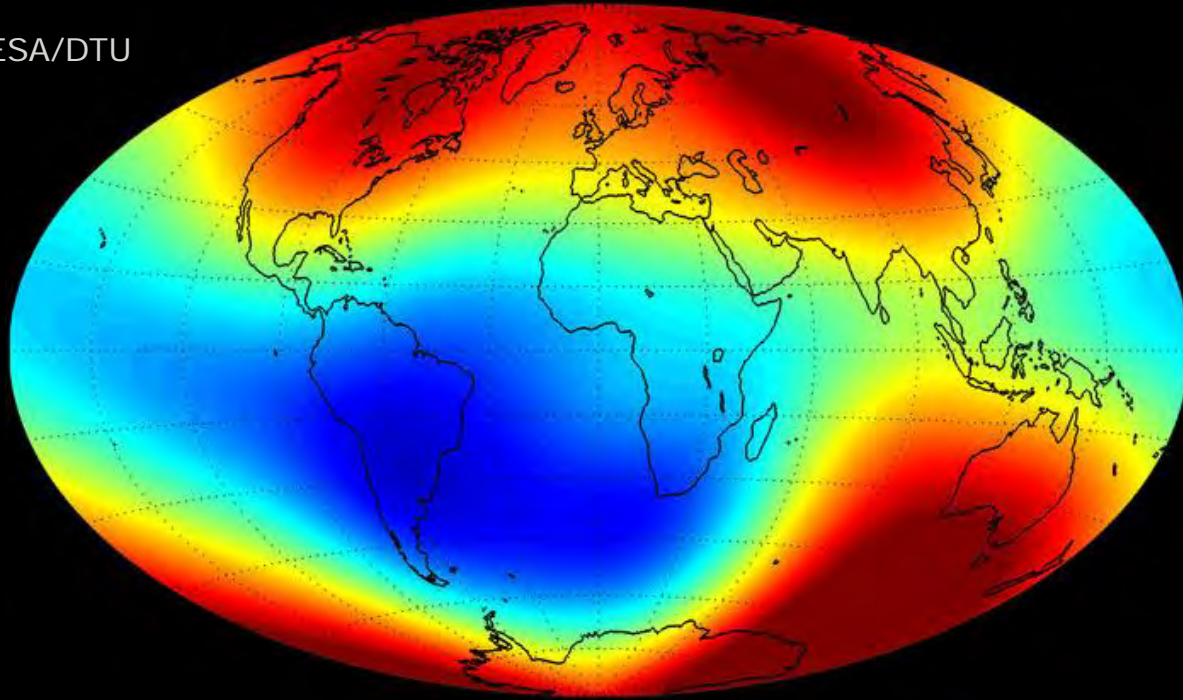


- Three-satellite-constellation, launched 22 November 2013
- Measures the geomagnetic field
- 4 yr nominal mission – until 2018

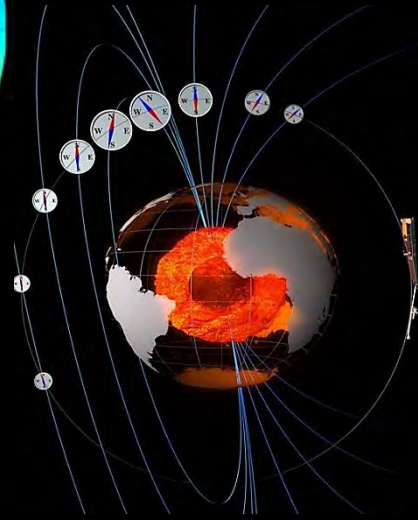
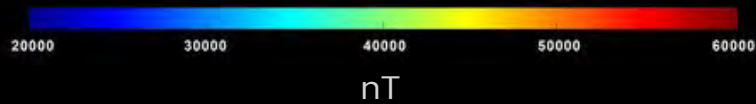


# Swarm: Earth's Magnetic Field

© ESA/DTU

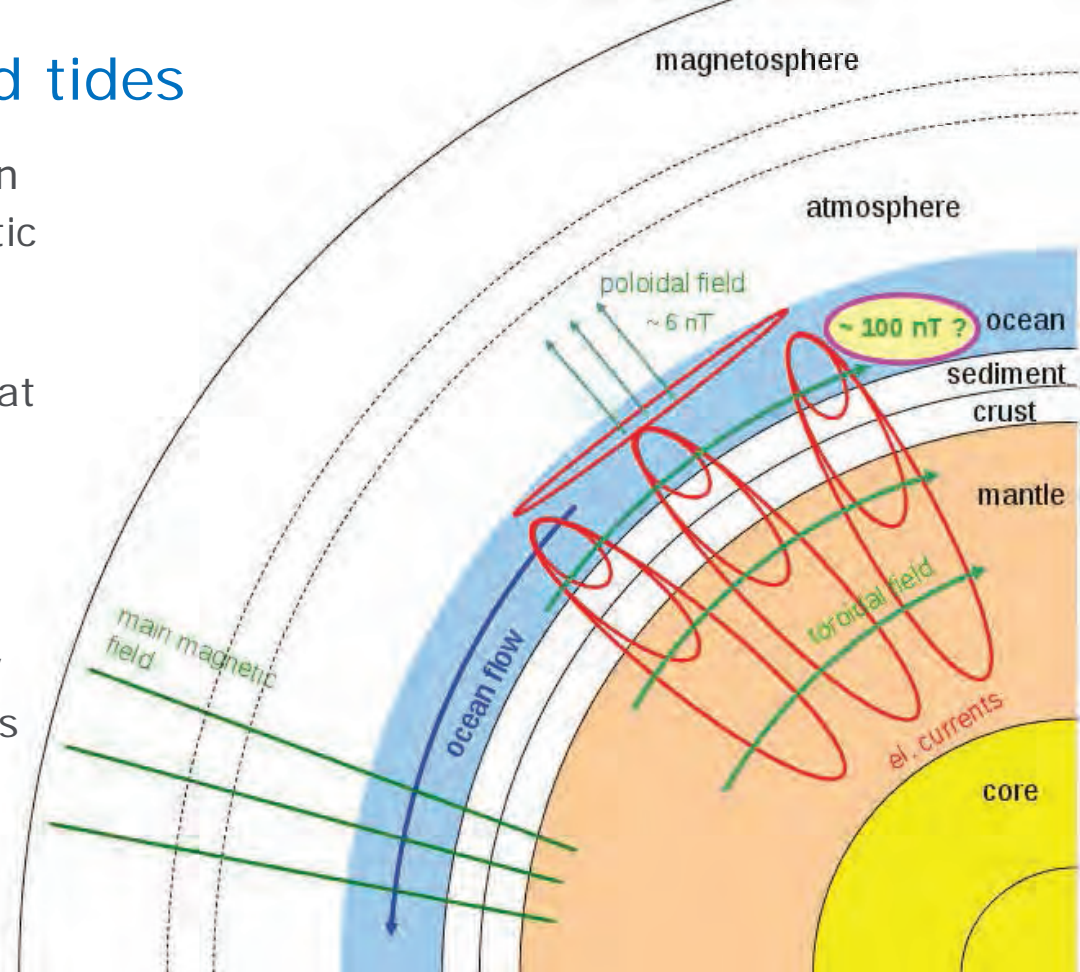


Main magnetic field at Earth's surface as of June 2014



# Swarm, ocean currents and tides

- ocean current moving in Earth's main magnetic field induce secondary magnetic fields: both poloidal and toroidal
- magnetic signatures are observable at sea-bottom, ocean-island, and coastal geomagnetic observatories, and newly also by low-orbit satellites
- Is it possible with Swarm to quantify the poloidal effects of the ocean using its magnetic field observations?
- Unique ocean observable related to integrated ocean water flow

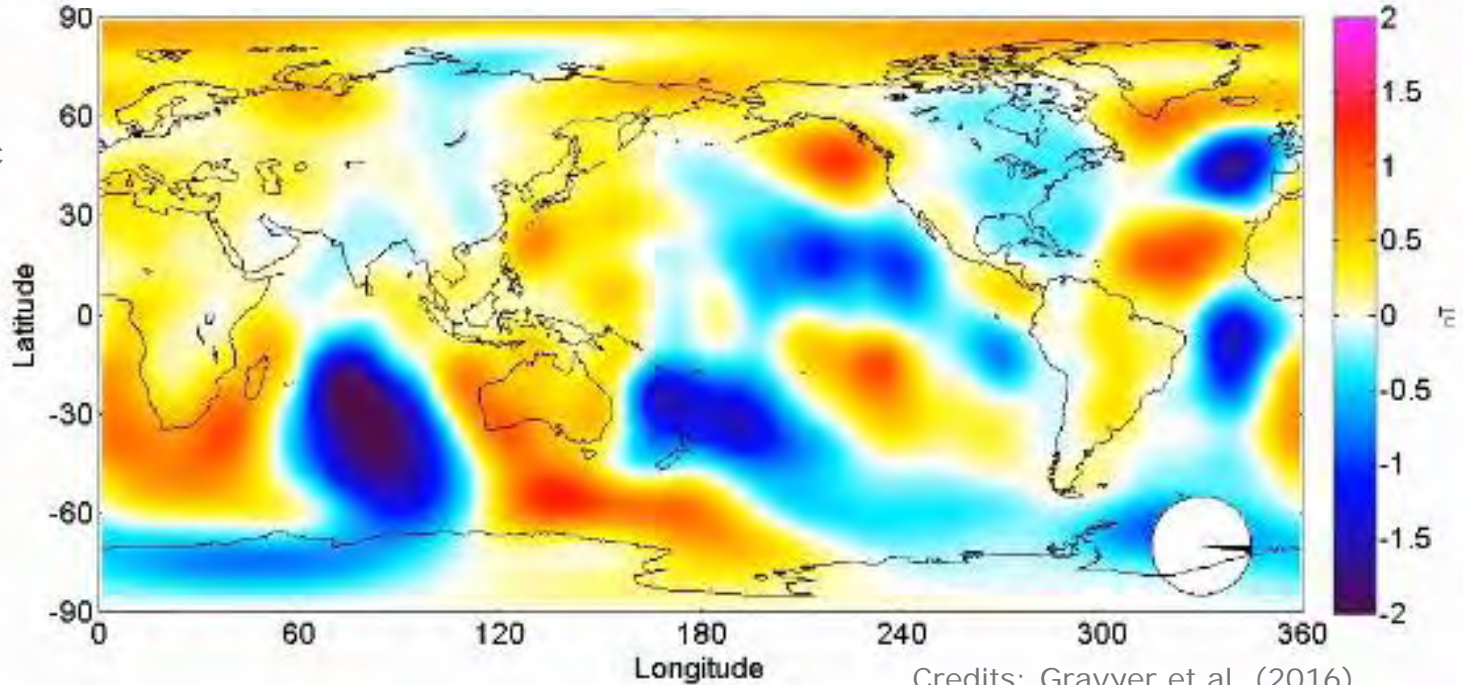


# Swarm, oceans and tides

This information has been used to estimate the conductivity in the asthenosphere (galvanic coupling)

→ Next step:  
How to estimate parameters related to ocean characteristics from Swarm?

## Swarm geo-magnetic signal from M2 tide mode



Credits: Gravyer et al. (2016)

RESEARCH ARTICLE

GEOPHYSICS

Satellite tidal magnetic signals constrain oceanic lithosphere-asthenosphere boundary

Alexander V. Grayver,<sup>1\*</sup> Neesha R. Schnepf,<sup>2</sup> Alexey V. Kuvshinov,<sup>1</sup> Terence J. Sabaka,<sup>3</sup> Chandrasekharan Manoj,<sup>4</sup> Nils Olsen<sup>5</sup>

The tidal flow of electrically conductive oceans through the geomagnetic field results in the generation of secondary magnetic signals, which provide information on the subsurface structure. Data from the new generation of satellites were shown to contain magnetic signals due to tidal flow; however, there are no reports that these signals have been used to infer subsurface structure. We use satellite-detected tidal magnetic fields to image the global electrical structure of the oceanic lithosphere and upper mantle down to a depth of about 250 km. The model derived from more than 12 years of satellite data reveals a ~72-km-thick upper resistive layer followed by a sharp increase in electrical conductivity likely associated with the lithosphere-asthenosphere boundary, which separates colder rigid oceanic plates from the ductile and hotter asthenosphere.

INTRODUCTION

Electrical conductivity (the reciprocal of resistivity) provides a wealth of information on the thermal and compositional state of Earth's mantle (1,2), with high sensitivity to small fractions of conductive phases, such as fluids and partial melts. Conventionally, the electrical structure of the oceanic lithosphere and upper mantle has been studied with seafloor magnetotelluric (MT) sounding using natural ionospheric excitation sources (3–5). Recent progress in the quality of satellite data, as well as processing and modeling techniques, now allows us to use another natural source: ocean tidal flow. Secondary electromagnetic (EM) fields produced by the electrically conductive seawater flowing through the ambient geomagnetic field obey Maxwell's equations

$$\begin{aligned} \mu^{-1} \nabla \times \vec{B} &= \alpha \vec{E} + \vec{j}^{\text{ext}} \\ \nabla \times \vec{E} &= \alpha \vec{B} \end{aligned} \quad (1)$$

where  $\vec{E}$  and  $\vec{B}$  are electric and magnetic fields, respectively;  $\mu$  and  $\alpha$  are magnetic permeability and electrical conductivity of the medium, respectively;  $\omega$  is the angular frequency; and  $\vec{j}^{\text{ext}}$  is the extraneous current due to tidal flow given by

$$\vec{j}^{\text{ext}} = \alpha (\vec{v} \times \vec{B}^{\text{main}}) \quad (2)$$

Here,  $\alpha$  is the conductivity of seawater (Fig. 1D),  $\vec{B}^{\text{main}}$  is Earth's main (core) magnetic field (Fig. 1, A to C), and  $\vec{v} = \vec{u}/h$ , where  $h$  is the height of the water column and  $\vec{u}$  is the depth-integrated seawater velocity due to tidal forces (Fig. 1, E and F)—a parameter that is well constrained by modern high-resolution assimilated global models of deep ocean tides (6, 7). In contrast to previous synthetic studies (8–10),

all quantities—including  $\alpha$ —in Eq. 2 vary laterally. The phenomenon described by Eqs. 1 and 2 is known as "motional induction" (11, 12).

It was shown that satellite data contain measurable magnetic signals due to tidal flow (8, 9), and these signals have sensitivity to subsurface structures (13). Attempts have been made to estimate bulk electrical properties of the subsurface using motionally induced EM signals recorded at isolated locations on land and on the seafloor (14, 15). These signals have also been used in ocean circulation studies (16), but their use for sounding Earth's conductivity was not reported to date.

Earth sounding with satellite-detected tidal magnetic signals differs from conventional EM sounding in several ways. Conventional methods, such as MT, rely on a broad frequency content of the detected natural EM variations, whereas the tidal signal is limited to the frequency of the corresponding tide. By analogy with techniques, such as electrical impedance tomography (17), the sounding is still possible because of the spatially heterogeneous nature of the extraneous currents generated in the oceans and because induced secondary magnetic fields can be detected at multiple locations (for instance, at satellites). Another distinguishing feature is the galvanic coupling of the oceans with the seafloor. Methods with a purely inductive excitation mechanism (based on EM variations in the ionosphere or magnetosphere) are generally weakly influenced by the toroidal part of the exciting field. This leads to reduced sensitivity for resistive structures in the subsurface (18). In contrast, detected tidal magnetic signals (14) include this component through galvanic coupling and interaction of the induced fields with lateral inhomogeneities.

RESULTS

The availability of more than 12 years of satellite and magnetic observational data (19) enabled us to robustly extract the magnetic field due to the principal lunar semidiurnal ( $M_2$ ) tidal constituent (Fig. 2A) as a data set with unprecedented globally uniform spatial coverage. At a satellite altitude of 430 km, the tidal field has a maximum amplitude of 2.1 nT, which is a relatively weak signal compared to the maximum total magnetic field intensity at that height (up to 54,000 nT). Nevertheless, observed tidal magnetic signals cannot be explained with

- Using the geo-magnetic signals from ocean tides Swarm data have been used to measure the electrical conductivity of the lithosphere-asthenosphere boundary
- The tidal flow of electrically conductive oceans through the geomagnetic field results in the generation of secondary magnetic signals, which provide information on the subsurface structure.
- The team – ETH (CH) and DTU (DK) used Swarm-based tidal magnetic fields to image the global electrical structure of the oceanic lithosphere and upper mantle down to a depth of about 250 km.
- The model derived from more than 12 years of satellite data (Swarm and Champ) reveals a ~72-km-thick upper resistive layer followed by a sharp increase in electrical conductivity likely associated with the lithosphere-asthenosphere boundary, which separates colder rigid oceanic plates from the ductile and hotter asthenosphere.

Figure: Amplitudes of the radial magnetic field components due to the M2 tide at an altitude of 430 km. (Top) Extracted from satellite data. (Below) Calculated on the basis of the recovered conductivity model.

Downloaded from <http://advances.sciencemag.org/> on October 4, 2018

<sup>1</sup>Institute of Geophysics, ETH Zürich, Sonneggstrasse 5, Zürich, Switzerland. <sup>2</sup>Department of Geological Sciences, Cooperative Institute for Research in Environmental Sciences (CIRES), University of Colorado, Boulder, CO 80505–3337, USA. <sup>3</sup>University of Maryland System, NASA/Goddard Space Flight Center, Greenbelt, MD, USA. <sup>4</sup>National Oceanic and Atmospheric Administration's National Centers for Environmental Information/CIRES, University of Colorado, Boulder, CO 80505–3338, USA. <sup>5</sup>DTU Space, Lyngby, Denmark. \*Corresponding author. Email: [agrayve@erdw.ethz.ch](mailto:agrayve@erdw.ethz.ch)

# Swarm: revealing earthquakes geo-magnetic footprint

Earth and Planetary Science Letters 461 (2017) 119–126



## Potential earthquake precursory pattern from space: The 2015 Nepal event as seen by magnetic Swarm satellites

A. De Santis<sup>a,b,\*</sup>, G. Balasis<sup>c</sup>, F.J. Pavón-Carrasco<sup>a,1</sup>, G. Cianchini<sup>a</sup>, M. Mandea<sup>d</sup>

<sup>a</sup> Istituto Nazionale di Geofisica e Vulcanologia, Rome, Italy

<sup>b</sup> G. D'Annunzio University, Chieti, Italy

<sup>c</sup> Institute for Astronomy, Astrophysics, Space Applications and Remote Sensing, National Observatory of Athens, Athens, Greece

<sup>d</sup> Centre National d'Etudes Spatiales, Paris, France

### ARTICLE INFO

Article history:  
Received 13 May 2016  
Received in revised form 22 September 2016  
Accepted 22 December 2016  
Available online xxxxx  
Editor: B. Buffet

Keywords:  
earthquake  
magnetic satellites  
Swarm  
lithosphere–atmosphere–ionosphere coupling

### ABSTRACT

A large earthquake of 7.8 magnitude occurred on 25 April 2015, 06:26 UTC, with the epicenter in Nepal. Here, taking advantage of measurements provided by the Swarm magnetic satellites, we investigate the possibility to detect some series of pre-earthquake magnetic anomalous signals, likely due to a lithosphere–atmosphere–ionosphere coupling, that can be a potential earthquake precursory pattern. Different techniques have been applied to Swarm data available during two months around earthquake occurrence. From the detected magnetic anomalies series (during night and magnetically quiet times or with an automatic detection algorithm), we show that the cumulative number of anomalies follows the same typical power-law behavior of a critical system approaching its critical time, and hence recovers as the typical recovery phase after a large event. The similarity of this behavior with the one obtained from seismic data analysis and the application of the analyses also to another period without significant seismicity do support a lithospheric-linked origin of the observed magnetic anomalies. We suggest that they might be connected to the preparation phase of the Nepal earthquake.

© 2017 Elsevier B.V. All rights reserved.

### 1. Introduction

The lithosphere, under the stress due to the plate tectonics, releases most of its energy with some rapid ruptures: the earthquakes (EQs). Intense shallow EQs are usually very destructive. Their seismic release requires a long time of preparation before it occurs so suddenly, when a particular fault cannot longer sustain the increasing deformation (e.g. Scholz, 2002). Recently, it has been shown that the ionosphere keeps the signature of seismic fault shortly after an earthquake (e.g. Ochiipinti et al., 2013, and references therein). This offers the possibility to retrieve seismic information from ionospheric observations.

An important and debated question arises about the possibility that, during the phase of EQ preparation, electromagnetic waves and/or particles could be transferred from the solid Earth (in particular the lithosphere) to the atmosphere, with a particular effect in the ionosphere, above around 50 km (e.g. Pulintets and Boyarchuk, 2004; Freund, 2011; Pulintets and Ouzounov, 2011;

De Santis et al., 2015). One of the most general models of coupling is based on the emission of a radioactive gas (Pulintets and Boyarchuk, 2004) or metallic ions (Freund, 2011) before a large earthquake, which may change the distribution of electric potential above the surface of the Earth and then up to the ionosphere (e.g. Pulintets and Boyarchuk, 2004; Sorokin et al., 2001). Penetration of the electric field to the ionosphere could produce ionospheric plasma density and/or conductivity anomalies, which are observed above seismic zones (e.g. Liu et al., 2006; Kon et al., 2011). An alternative explanation is that the radon emitted before an earthquake would increase the conductivity of air at ground level and that the ensuing increase of current in the fair weather global circuit would lower the ionosphere (Harrison et al., 2010). Therefore, it is expected that low Earth orbiting (LEO) satellites could be the best possible dedicated platforms of sensors to detect any electromagnetic, acoustic or infrared seismic-linked precursors. Certainly, space observations have to be investigated together with ground (and near-surface) seismic and other geophysical observations, in order to have a more complete picture of the possible involved phenomena.

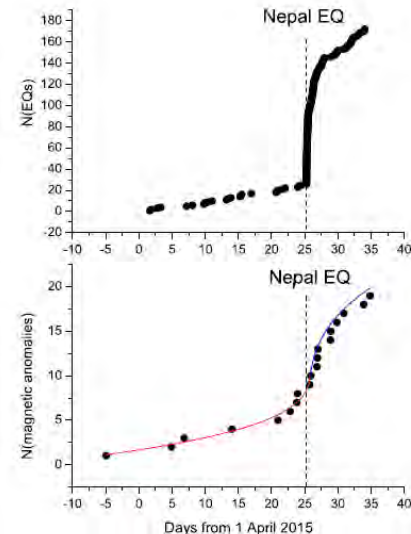
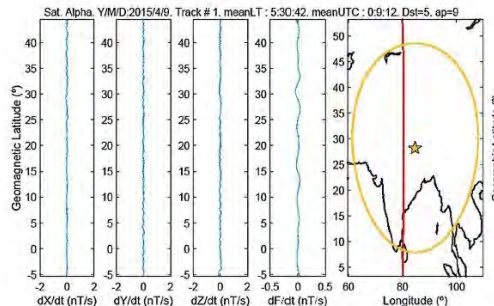
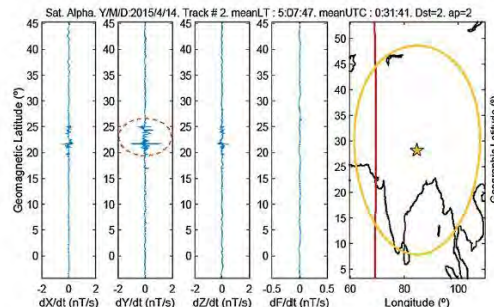
Few attempts have been made to deeply investigate pre-EQ ionospheric perturbations. The French satellite mission, DEMETER (Detection of Electro-Magnetic Emissions Transmitted from Earthquake Regions), was suitably designed and launched (2004–2010)

\* Corresponding author at: Istituto Nazionale di Geofisica e Vulcanologia, Rome, Italy.

E-mail address: angelo.deantis@ingv.it (A. De Santis).

<sup>1</sup> Now at: Universidad Complutense de Madrid, Madrid, Spain.

<http://dx.doi.org/10.1016/j.epsl.2016.12.017>  
0012-821X/© 2017 Elsevier B.V. All rights reserved.



**Top: Cumulative number of M4+ earthquakes occurred within Dobrovolsky area versus time**

**Bottom: Cumulative number of magnetic anomalies detected by Swarm satellite A versus time.**

**An example of chosen track with an anomaly (top) and (bottom) without significant anomalies. The start shows the epicenter of the earthquake.**

**Source: INGV (IT)**



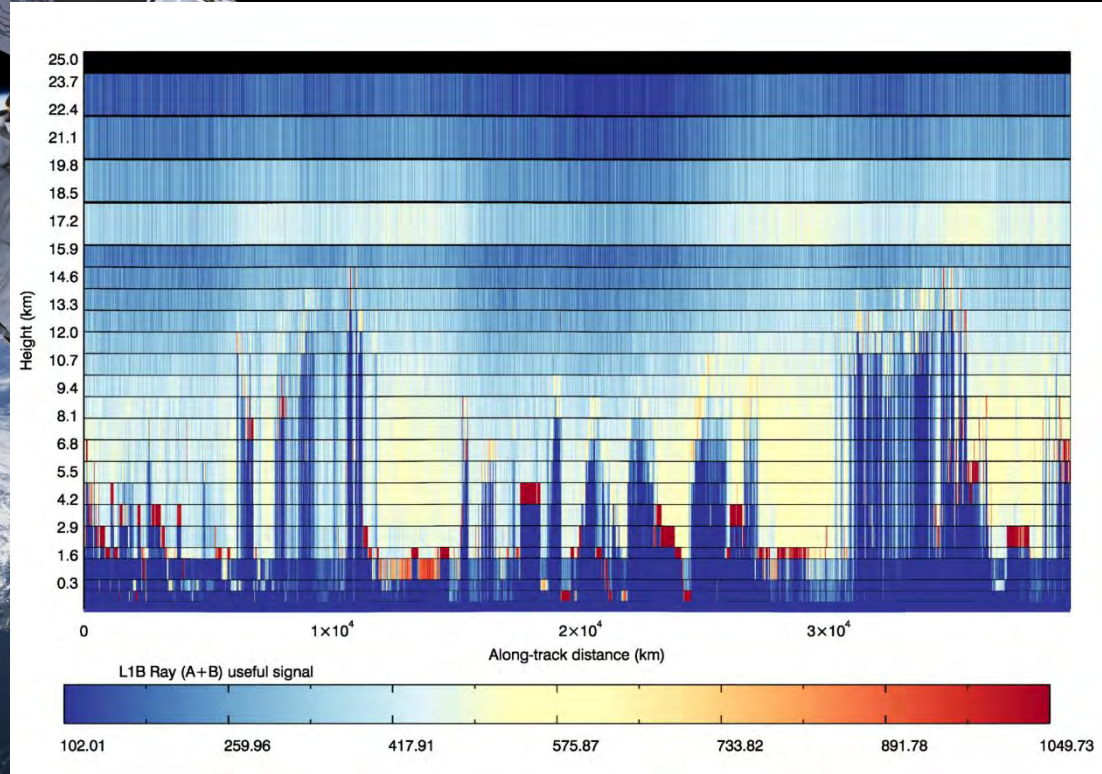
# Successfully Launched

- Observations of wind profiles for analysis of global wind field
- Doppler UV lidar (355 nm) with Mie and Rayleigh receivers
- Doppler shift used to retrieve Horizontal Line of Sight component of wind velocity
- Understanding of atmosphere dynamics and climate processes
- Improved weather forecasts and climate models

# Aeolus



- Successful launch the 22 August
- Image shows backscattered light from air molecules, cloud tops and the ground (very first signal).
- Light blue and yellow colours indicate areas that are cloud-free, darker yellow and red indicate dust particles, thin and thicker clouds, and in some cases red also indicates Earth's surface. Darker blue indicates areas where the ultraviolet light has travelled through a cloud or where there is no signal.



ESA's sixth Earth Explorer Mission,  
implemented in cooperation with JAXA

Mission goal: relationship of  
clouds, aerosol and  
radiation budget

Launch: Soyuz 2020

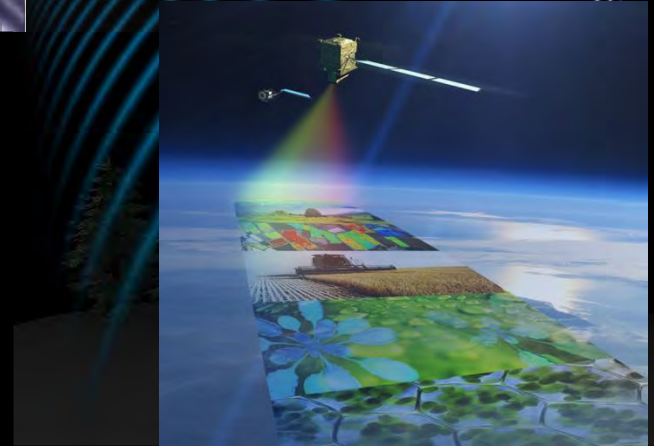
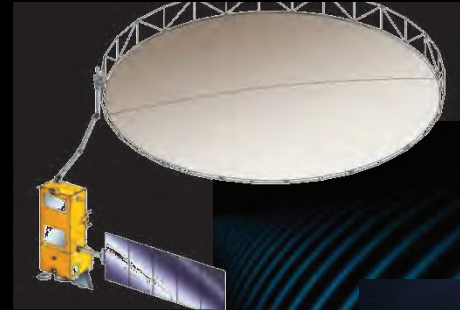


ESA: satellite, launch, operations,  
3 instruments (ATLID, MSI, BBR)

JAXA: cloud profiling radar

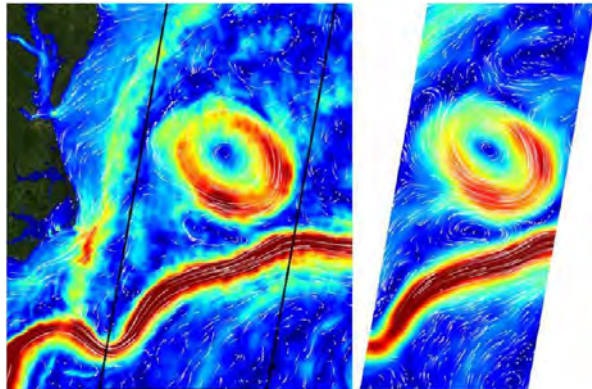
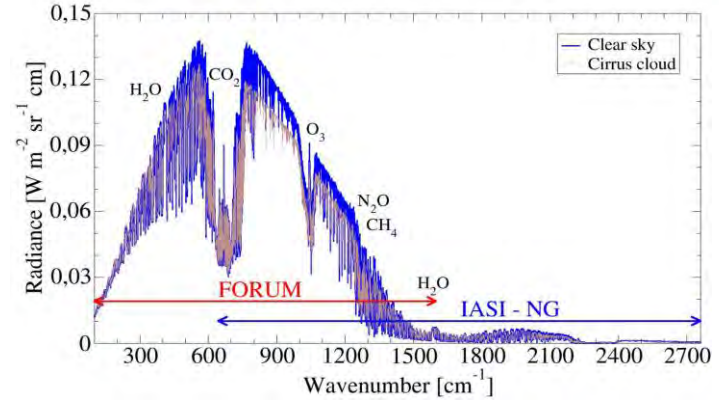
# Further Earth Explorer Missions

- 7<sup>th</sup> Earth Explorer: Biomass
  - Biomass estimates based on global interferometric and polarimetric P-Band Radar observations
  - Launch: 2021 (Vega)
- 8<sup>th</sup> Earth Explorer: FLEX
  - global maps of vegetation fluorescence, which can be converted into an indicator of photosynthetic activity
  - Launch: 2022 (Vega)



# Candidate Earth Explorer - 9

**FORUM: Far-infrared-Outgoing-Radiation Understanding and Monitoring** will provide the first global, spectrally resolved observations of the outgoing longwave radiation from  $100$  to  $1600\text{ cm}^{-1}$  ( $100 - 6.25\text{ }\mu\text{m}$ ) with a resolution of  $0.3\text{ cm}^{-1}$  and  $0.1\text{ K}$  accuracy to improve climate models.



modeled current ("truth")

SKIM L3A

**SKIM: Sea surface Kinematics Multiscale monitoring** will measure total ocean surface velocity vector using a high-resolution Ka-band Doppler altimeter, measuring at nadir and rotating off-nadir beams ( $0, 6$  and  $12^\circ$  incidence angles) providing accuracy on horizontal current velocity is  $0.1\text{ m/s}$ , at a resolution of about  $40\text{ km}$  with swath of  $270\text{ km}$  and coverage up to  $82^\circ\text{ N}$ .

European Space Agency

